



Review

Iron Oxide Nanoparticles: An Alternative for Positive Contrast in Magnetic Resonance Imaging

Irene Fernández-Barahona ^{1,2,†} , María Muñoz-Hernando ^{1,3,†} , Jesus Ruiz-Cabello ^{2,4,5,6} ,
Fernando Herranz ^{1,4} and Juan Pellico ^{4,7,*}

¹ NanoMedMol Group, Instituto de Química Medica (IQM), Consejo Superior de Investigaciones Científicas (CSIC), 28006 Madrid, Spain; ifernandezbarahona@ucm.es (I.F.-B.); maria.munoz@cnic.es (M.M.-H.); fherranz@iqm.csic.es (F.H.)

² Facultad de Farmacia, Universidad Complutense de Madrid, 28040 Madrid, Spain; jruizcabello@cicbiomagune.es

³ Centro Nacional de Investigaciones Cardiovasculares Carlos III (CNIC), 28029 Madrid, Spain

⁴ Ciber de Enfermedades Respiratorias (CIBERES), 28029 Madrid, Spain

⁵ Center for Cooperative Research in Biomaterials (CIC biomaGUNE), Basque Research and Technology Alliance (BRTA), 20014 Donostia San Sebastián, Spain

⁶ IKERBASQUE, Basque Foundation for Science, 48013 Bilbao, Spain

⁷ School of Biomedical Engineering & Imaging Sciences, King's College London, St. Thomas' Hospital, London SE1 7EH, UK

* Correspondence: juan.pellico@kcl.ac.uk; Tel.: +44-(0)-7712870441

† These authors contributed equally to this work.

Received: 31 March 2020; Accepted: 8 April 2020; Published: 10 April 2020



Abstract: Iron oxide nanoparticles have been extensively utilised as negative (T_2) contrast agents in magnetic resonance imaging. In the past few years, researchers have also exploited their application as positive (T_1) contrast agents to overcome the limitation of traditional Gd^{3+} contrast agents. To provide T_1 contrast, these particles must present certain physicochemical properties with control over the size, morphology and surface of the particles. In this review, we summarise the reported T_1 iron oxide nanoparticles and critically revise their properties, synthetic protocols and application, not only in MRI but also in multimodal imaging. In addition, we briefly summarise the most important nanoparticulate Gd and Mn agents to evaluate whether T_1 iron oxide nanoparticles can reach Gd/Mn contrast capabilities.

Keywords: iron oxide nanoparticles; magnetic resonance imaging; positive contrast agents

1. Introduction

Iron oxide nanoparticles (IONPs) are one of the most used nanomaterials in biomedicine. Among the reasons justifying this interest, their biocompatibility and magnetic properties are probably the most important. These properties have boosted their use in hyperthermia cancer treatment and, as imaging probes, in magnetic resonance imaging (MRI). When IONPs are prepared using “traditional” synthetic methods they show superparamagnetic properties. In other words, these nanoparticles show a very strong magnetic response when placed under the influence of a magnetic field, turning to zero when the magnetic field is off. Because of this, when placed inside MRI equipment, IONPs act as “small magnets”, suppressing the signal and, therefore, appearing as a dark spot, the so-called negative contrast. Due to the strong magnetic response, the concentration needed for an in vivo application is often low. However, based on this, IONPs have been, for a long time, the never fulfilled eternal promise to change the current clinical scenario in MRI. Currently, Gd-based compounds are the standard probes when an MRI scan is performed. It is well-known that, under certain circumstances, Gd compounds

show important toxicity. This is particularly important for patients suffering from kidney problems. Besides the toxicity problems, Gd probes normally have a small molecular weight and are, after injection, rapidly extravasated, excluding them from many applications that require long circulating times. If Gd-based probes present these problems, why have IONPs not displaced them from clinical practice? Basically, because the signal provided by Gd compounds is much more useful for in vivo diagnosis than that provided by IONPs for many diseases. This is due to the dark, negative signal that traditional IONPs generate. Frequently, in many diseases, hypointense (dark) areas appear naturally in an MR image. If the image probe generates a dark signal over a dark background, diagnosis gets complicated. For this reason, in recent years, researchers have searched for an alternative that can join the good physicochemical properties of IONPs with the outstanding imaging properties of Gd compounds. This has led to numerous synthetic developments producing extremely small iron oxide nanoparticles that, being more paramagnetic than superparamagnetic, are capable of generating bright, positive contrast in MRI. Here, we will critically review these developments, highlighting achievements and considering what is left to accomplish to reach a point at which the use of IONPs in clinics is as frequent as the use of gadolinium compounds.

2. T_1 -BASED MR

2.1. Spin Density and Relaxation Times

Magnetic resonance imaging (MRI) uses differences in spin density or relaxation properties (T_1 , longitudinal or spin lattice relaxation time, T_2 , transversal or spin-spin relaxation time, T_2^* , apparent transversal relaxation time) to generate signal-to-noise ratio and contrast between different soft tissues in an image. Apart from these relaxation times that are interrogating different features of molecular dynamics and physical mechanisms, each soft tissue (liver, brain, heart, lung, etc.) will have a different chemical composition and different spin densities to encode an image using MRI. Water or fat are the usual predominant content of tissues; therefore, spin densities of tissues are often given by the concentration of water weighted by the relaxation properties and the acquisition parameters and type of sequence used. T_1 is normally much longer than T_2 and does not exhibit proportionality among them. Table 1 shows typical relaxation time values for different tissues at normal magnetic fields for clinical applications.

Table 1. Typical relaxation times values of some tissues at clinical magnetic fields.

		1.5 T		3 T	
Tissue		T_1 (ms)	T_2 (ms)	T_1 (ms)	T_2 (ms)
Brain	Grey matter	1150	100	1600	70
	White matter	800	80	1100	60
	CSF	4500	2200		
Skeletal muscle		1000	35	1400	30
Fat		250	60		
Blood		1400	290	1900	275
Liver		580	55	810	56
Cardiac muscle		1030	42	1400	47

2.2. T_1 -Weighted or Positive Contrast Using Gradient and Spin Echo Sequences

For T_1 -contrast, imaging is performed by emphasising the differences in longitudinal components of magnetisation. This information can be coded with typical spin-echo or gradient-echo sequences. In the spin-echo sequences, two radiofrequency (RF) pulses (one at 90° followed by another at 180° or refocusing pulse) are used to acquire the signal. T_1 -weighted imaging in a spin-echo sequence is determined by the repetition time (i.e., the temporal distance between two consecutive 90-degree pulses, also called T_R) whilst echo times (named T_E hereinafter) are kept at the lowest possible value. The spin-echo sequences have the value of being immune to off-resonance artefacts caused by B_0

inhomogeneities and to magnetic susceptibility shifts due to heterogenous tissues (such as multiple air-tissue interfaces in lung tissue or in some brain or abdominal regions) or to the presence of magnetic impurities (such as the presence of iron oxide nanoparticles).

In contrast to this alternative, a gradient-echo [1] image is formed with a single pulse (flip angle (θ) generally inferior to 90°), combined with the application of two lobes, also called dephasing and rephasing gradients, and the absence of a 180° refocusing pulse, per each RF excitation. Differently to the spin-echo methods, local susceptibilities are not refocused in this approach, so image quality is normally inferior and signal reduction is anticipated at gradient-echo sequences.

For our purpose here, to help to understand the contents of this review, for T_1 -contrast or positive contrast with nanoparticles, keeping a short T_E in the pulse sequence should not be a problem for most MRI systems. Longer T_E enables a T_2^* weighting contrast, which for certain nanoparticles can still be recommendable. However, for positive contrast or T_1 -contrast, T_E should be kept as short as possible. The selection of the best θ to maximise the T_1 contrast will then be critical for final optimisation. This flip angle finally enables T_1 weighting and must be investigated to allow fast imaging (short T_R) with this possibility. To do so, we need to take into consideration the expected T_1 and T_2 values of the different tissues for the magnetic field used in the study (see Table 1). As we can see from this table, T_1 values generally will increase with B_0 , whereas T_2 remain constant, so the properties as contrast agent are normally very different at low (<1.5 T) and high fields (>3 T).

3. Nanoparticles for Positive Contrast MRI

Despite the high resolution of anatomical features presented by MRI, sensitivity is one of the weak points. MRI relies on the differences in tissue proton density and therefore differences in tissues' relaxation times to generate contrast. These differences allow discrimination between bone, air, and soft tissues in vivo. Nevertheless, discrimination of certain tissues and diseased areas gets complicated when these differences do not generate enough contrast. For this reason, contrast agents are regularly used to facilitate the diagnosis and characterisation of pathologies at cellular and molecular levels [2]. T_1 or positive contrast agents shorten the longitudinal relaxation time in the areas or tissues where accumulation occurs, making brighter images. The majority of clinically available T_1 contrast agents are paramagnetic metallo-chelates, composed of Gd, whose potential toxicity and short circulating times have driven the quest for improved positive contrast agents that overcome these limitations [3].

Nanostructured materials exhibit unique properties by virtue of their size. At this scale, quantum effects dominate material behaviour, conferring the size-dependent magnetic, electrical and optical behavior of nanomaterials. At the nanoscale, materials present an enhanced surface-to-volume ratio, extremely useful for bioconjugation purposes and targeted imaging. There is a broad variety of nanoparticulate T_1 contrast agents mainly based on the incorporation of paramagnetic Gd or Mn (Table 2). Some of the most remarkable are summarised below.

3.1. Paramagnetic Gd_2O_3 Nanoparticles

Gadolinium-based contrast agents are the gold standard T_1 contrast agents for MRI; however, their toxicity and reduced number of applications boosted the quest for alternatives. Most of Gd-based T_1 contrast agents are based on organic molecules chelating Gd^{3+} ions to prevent toxicity. However, inorganic nanoparticles made up of Gd are increasingly common. Gadolinium oxide [4,5], gadolinium fluoride [6,7] and gadolinium phosphate [8] NPs have been synthesised and tried as T_1 contrast agents. Most recent examples are focused on targeted T_1 Gd_2O_3 NPs [9], dual T_1 - T_2 MRI probes [10], hybrid MRI/fluorescent probes [11,12] and theranostic (therapy + diagnostic) probes [13] for tumour imaging. A Gd_2O_3 -NP hybrid CT/MRI probe functionalised with bisphosphonate was used by Mastrogriaco et al. to visualise calcium phosphate bone cement [14]. Dai et al. carried out a comparison between their PEGylated- Gd_2O_3 nanoparticles and the commercially available Magnevist, observing that their NPs presented a long half-life in blood and efficient MRI contrast, lower hepatic and renal toxicity and greater accumulation at the tumour site [15].

3.2. Paramagnetic MnO Nanoparticles

Manganese ions have emerged as a potential alternative to gadolinium as T_1 enhancer; however, their toxicity, affecting the central nervous and the cardiovascular systems, has determined its clinical application [16,17]. Manganese oxide nanoparticles have emerged as the most suitable alternative to overcome these toxicity issues [18]. Size and shape control allow fine tuning of the relaxivity values of these nanoparticles. PEGylated MnO NPs have been demonstrated by several groups to be useful and non-toxic T_1 contrast agents [19,20]. Their use for tumour detection is fairly popular, both in a non-specific and specific manner. Wang et al. achieved MnO NP accumulation in gliomas by elongating the circulation time of their MnO NPs, functionalising their surface with cysteine [21]. Chen et al. also managed to visualise mouse gliomas using MnO NPs, however using a glioma-specific moiety: folic acid [22]. Gallo et al. achieved M21 tumour visualisation in mice using RGD (arginine-glycine-aspartate peptide)-functionalised MnO nanoparticles [23]. Renal carcinoma T_1 MR imaging was accomplished by Li et al., targeting MnO NPs using AS1411 aptamer [24]. Manganese oxide NPs have also been used as theranostic platforms for drug delivery and photothermal therapy at the tumour site [25–27]. MnO NPs have served as a platform to synthesise hybrid molecular imaging probes for both PET (Positron Emission Tomography)/MRI for tumour vasculature imaging using ^{64}Cu [28] and fluorescence/MRI with Cy7.5 for lymph node mapping [29].

3.3. Organic Nanostructured Materials

Organic nanostructured materials have a long history as contrast agents for MRI. However, their use has been limited, as the relaxivity values of most of them, such as albumin- and dextran-based MR probes, are often insufficiently high.

Dendrimers are polymeric molecules with monomers branching out radially from a central core, forming a tree-like architecture [30]. As their synthesis is stepwise, resultant structures present narrow polydispersity, and terminal groups on the surface of the dendrimer can be included in a controlled manner [31]. The most commonly used monomers are polyamidoamine (PAMAM), polypropylimine (PPI), poly(ether imine) (PETIM) and poly-L-lysine (PLL) [32]. Due to plentiful anchoring sites for paramagnetic ions in their structure, they are appropriate nanoplatforms to integrate paramagnetic ions in their structure. Gadolinium (Gd^{3+}) is one of the most repeatedly used ions in dendrimers for T_1 MRI. The macromolecular size of these ions increases the rotational correlation times of integrated Gd^{3+} , resulting in relaxivities larger than most of the clinically approved Gd-based contrast agents with low molecular weight. The use of these macromolecular probes has been demonstrated in lymphatic imaging [33], tumour detection [34], liver fibrosis staging [35], and colon cancer and brain theranostics [36]. Mn^{2+} -based compounds have been also proposed as non-toxic alternatives to Gd chelates to image hepatocellular carcinoma and atherosclerosis [37,38]. Fan et al. have recently shown that Cu^{2+} can be integrated in dendrimeric structures to form a platform for tumour/metastasis imaging and chemotherapy [39].

3.4. Silica Based Nanoparticles

One of the main applications for SiO_2 nanoparticles is drug delivery that, combined with the possibility of carrying paramagnetic ions in their pores or surface, yields excellent theranostic agents. Kim et al. used Mn-doped silica NPs to detect hepatocellular carcinoma [40]. Li et al. made use of a theranostic agent based on mesoporous manganese silica NPs loaded with doxorubicin to image and treat a breast cancer xenograft murine model [41]. Gd^{3+} -containing silica NPs have also been used in vivo and/or in vitro as a T_1 contrast agent [42–44]. Recently, Carniato et al. summarised the most remarkable examples of Gd-based mesoporous silica nanoparticles for MRI. In this work, the influence over the relaxometric properties of important factors such as the porosity, the localisation of the paramagnetic chelate and the surface properties of the mesoporous silica nanoparticles are discussed in detail [45]. For instance, Davis et al. reported mesoporous silica nanoparticles doped with Gd in the inner or outer part of the pore and in the surface of the particle showing great differences in the relaxivity values depending on the Gd localisation [46].

Table 2. Composition, hydrodynamic diameter (D_H , nm) and r_1 ($\text{mM}^{-1} \text{s}^{-1}$) at magnetic field B_0 (T) of some reported T_1 based nanoparticles.

Nanomaterial	Composition	D_H Size (nm)	r_1 ($\text{mM}^{-1} \text{s}^{-1}$)	B_0 (T)	Ref.
Paramagnetic inorganic NPs-Gadolinium	Core-shell Gd_2O_3 @polisiloxane	3.3 ± 0.8	8.8	7	[4]
	D-glucuronic acid-coated Gd_2O_3	1	9.9	1.5	[5]
	Citrate-coated GdF_3 , AEP-coated $\text{GdF}_3/\text{LaF}_3$	129.3	8.8 ± 0.2	3	[6]
	PAA ₂₅ -stabilized $\text{GdF}_3/\text{CeF}_3$ NPs	70	40 ± 2	1.5	[7]
	PGP/dextran-K01	23.2 ± 7.8	13.9	0.5	[8]
	ES-GON-PAA	<2	70.2 ± 1.8	1.5	[9]
	Gd_2O_3 @PCD-FA	131 ± 4.6	3.95	3	[10]
	Gd_2O_3 -FI-PEG-BBN	52.3	4.23	3	[13]
	Bisphosphonate-functionalised Gd_2O_3	70	15.41	3	[14]
Paramagnetic inorganic NPs-Manganese	PEG- Gd_2O_3	36.35 ± 1.9	29	3	[15]
	MnO @PDn	24.8 ± 0.2	4.4	1.41	[19]
	mPEG-SA-dopamine-MnO	120	16.14	3	[20]
	L-cysteine-functionalised PEG-coated Mn_3O_4	213.3 ± 2.4	3.66	0.5	[21]
	FA-TETT-MnO	122	4.83	7	[22]
	MnO @AUA@PEG ₅₀₀₀ @RGD	56.7 ± 13.2	1.44	9.4	[23]
	PEG-MnO	15.08 ± 2.7	12.94	3	[24]
	Mn-LDH	48	9.48	-	[25]
	MnCO_3 @polydopamine	173	8.3	7	[27]
Dendrimers	NOTA- Mn_3O_4 @PEG-TRC105	32.6 ± 4.5	0.54	4.7	[28]
	Mn_3O_4 @PEG-Cy _{7.5}	10 ± 2.3	0.53	7	[29]
	PAMAM G5-BnDOTA-Gd	6.5	12.98	3	[33]
	Folic acid-G5-DOTA-Gd	-	26 ± 0.06	2	[34]
	Den-cRGD-DOTA-Gd	13.2	7.1 ± 0.3	4.7	[35]
	Gd^{3+} -G ₂ -Gd-Asparagine	90		1.5	[36]
	(Au) ₁₀₀ G5.NH ₂ -FI-DOTA(Mn)-HA	245.3	5.42	0.5	[37]
	PAMAM G8-DTPA-Mn	13.3 ± 1.2	3.5 ± 0.1	1.5	[38]
	G5.NHAc-Pyr/Cu(II)	153.2 ± 4.6	0.7024	0.5	[39]
Liposomes	DPPC/DPPG Gd-Liposomes	72 ± 6	1.13	0.5	[47]
	MCO-I-68-Gd/DNA liposomes	150			[48]
	Mab-Gd-SLs	129.9 ± 40.9	8.06	1.5	[49]
	RGD- and ATWLPPR- functionalised Gd-liposomes	89.9	~6	3	[50]
	RGD-CPGd-L	128	4.24	11.7	[51]
	THI0567-targeted liposomal-Gd	150–250	$2 \times 10^5/\text{particle}$	1	[52]
Silica NPs	Mn-SiO ₂	25 ± 2	6.7	3	[40]
	Doxorubicin-loaded SiO ₂ @MnSiO ₃	150	4.34	3	[41]
	Silyated Gd complex-coated [Ru(bpy) ₃]Cl ₂	37	19.7	3	[53]
	Gd-Si-DTTA	75	28.8	3	[44]
	Gd-DOTA-MSNs	66.3 ± 6.6	33.57 ± 1.29	7	[46]
	Gd-DTPA-334	20 ± 2	18.7	0.5	[54]
Carbon nanotubes (CNTs)	SRPs	8.3	11.9	1.5	[55]
	Gd ultrashort single-walled CNTs	-	90	1.5	[56]
	Gd-MWNT	-	6.61	7	[57]
	PAA-GNTs	-	150	1.5	[58]
Metal-organic frameworks (MOFs)	MWNT/GdL	-	50.3	0.5	[59]
	Eu-, Gd-, Tb- doped MOFs	100×35	35.8	3	[60]
	Core-shell PB@MIL-100(Fe)	100	1.3	3	[61]
	C(RGDfK)-MnMOFs	$50-100 \times 750$	4.0	9.4	[62]
	PCN-222(Mn)	241	35.3	1	[63]

3.5. Liposomes

Liposomes are spherical structures formed by one or several concentric lipid bilayers with an aqueous phase inside [64]. Due to their amphiphilic composition, they can integrate hydrophobic and/or hydrophilic molecules. This, added to their outstanding biocompatibility, has boosted their use as nanocarriers in drug delivery and molecular imaging. There are numerous examples of liposome-based MRI probes carrying paramagnetic agents, mostly composed of Gd^{3+} and Mn^{2+} in the

aqueous lumen [47,65–68]. Alternatively, some other liposomal contrast agents used in MRI carry the paramagnetic molecule in their lipid bilayer [48,69–72]. Recent applications of these probes include imaging of tumours [49–51,73], atherosclerotic plaque [52] and blood brain barrier permeability [74].

4. Iron Oxide Nanoparticles for MRI

Iron oxide nanoparticles have been mostly used as negative (T_2) contrast agent. Their superparamagnetic behaviour, driven by the magnetic mono-domains at nanometric scale in the appropriate iron oxide phase, along with the great saturation magnetisation values, provide excellent T_2 shortening in MRI images [75]. The limitations of T_2 -driven diagnosis has stimulated the development of iron oxide-based T_1 agents [76]. IONPs act as T_1 agent when certain physicochemical properties are fulfilled. These features, along with the synthetic method to achieve them, are summarised below.

4.1. Physicochemical Properties

IONP components, the core and coating, play an important role in the contrast behaviour. The composition, size and shape of both components must be controlled since they determine the iron oxide phase, crystallinity, magnetic properties and the hydrodynamic size. All of these properties are key to develop an IONP-based T_1 contrast agent.

In terms of size, we have to consider both the size of the core and the hydrodynamic size (core + coating). As a rule of thumb, in IONPs, the smaller the core the better the positive contrast. When the core size is decreased (<5 nm) the magnetic single domains decrease, leading to a spin canting effect, which provides five oriented and unpaired $\text{Fe}^{3+}/\text{Fe}^{2+}$ electrons, making the particle more paramagnetic than superparamagnetic (Figure 1). Smaller cores usually imply less crystallinity, with a subsequent decrease in the saturation magnetisation values (similar to paramagnetic materials). Therefore, maghemite ($\gamma\text{-Fe}_2\text{O}_3$) is often preferred for T_1 contrast rather than magnetite (Fe_3O_4) where the crystallinity is usually higher.

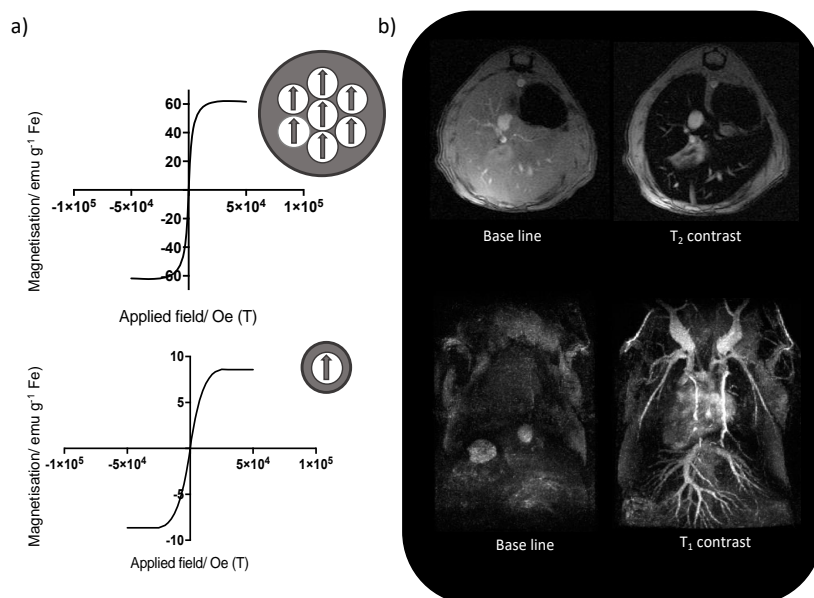


Figure 1. (a) Change in the magnetic behaviour of iron oxide nanoparticles with the decrease of the core size, from superparamagnetic (top) to paramagnetic (bottom), (b) Mouse liver T_2 -weighted MRI using iron oxide nanoparticles with bigger core size (top), T_1 -weighted MR angiography using iron oxide nanoparticles with smaller core sizes (bottom).

Core size and composition are essential but so is an appropriate coating. The stability of the nanoparticles is crucial to avoid aggregation, which triggers multiple particles to act as a single magnetic

domain and, hence, increases the T_2 effect. In this regard, different coatings such as small molecules, macromolecules or proteins have served as stabilisers [77–80]. In addition, the size of the coating has been demonstrated to be a key factor in the T_1 effect [81]. Large size coatings (i.e., large hydrodynamic size, >30–40 nm) restrict water access to the nanoparticle core increasing the outer-sphere contribution to the relaxation mechanism. Coatings providing ultrasmall hydrodynamic sizes (<7 nm) usually confer poor stability, with aggregation increasing the T_2 effect. This is, however, an interesting challenge due to the renal clearance of ultrasmall IONPs, which increase their translational potential. Coatings rendering medium hydrodynamic sizes (10–20 nm) provide good colloidal stability with a thin coating that increases the water exchange rate, boosting the T_1 effect.

Although these are general considerations, there is no general rule established to describe the best-case scenario for each T_1 -IONP. An optimal T_1 -weighted sequence, taking into account the physicochemical and relaxometric properties of the nanoparticles and selecting the experimental parameters to highlight them appropriately for each magnetic field, is mandatory. A great number of works have shown a wide variety of formulations, sizes and coatings with the magnetic field, pulse sequences, and acquisition parameters not always optimised for T_1 -weighted imaging. Table 3 summarises some of the reported T_1 -IONPs, depicting these differences and the influence over the relaxometric properties.

Table 3. Hydrodynamic diameter (D_H , nm), core size (nm) and r_1 , r_2 ($\text{mM}^{-1} \text{s}^{-1}$) at magnetic field B_0 (T) of reported T_1 -IONPs.

Sample	D_H (nm)	Core Size (nm)	r_1 ($\text{mM}^{-1} \text{s}^{-1}$)	r_2 ($\text{mM}^{-1} \text{s}^{-1}$)	B_0 (T)	(ref)
Cubic IONP	18	11	3.4	36.8	3	[82]
MDBC-USPIO	24	3.4	4.8	22.56	1.5	[83]
Pegylated SPIONs	10.1	5.4	19.7	39.5	1.5	[84]
$\text{Fe}_3\text{O}_4/\text{SiO}_2$	30–40	4	1.2	7.8	3	[85]
SPION	20 ± 7	5–10	13.31	40.90	1.4	[86]
ESIONs	-	3	4.78	29.25	3	[87]
IONAs	17	9	5.1	21.3	3	[88]
Cat-MDBC/USNP	20	3.4 ± 1.8	6.8	37.1	1.4	[89]
UMIONs	7.5	3.3 ± 0.5	8.3	35.1	4.7	[90]
GSH-IO NPs	4.19 ± 0.31	3.72 ± 0.12	3.63	8.28	4.7	[91]
Fe_3O_4 -PEG-RGD	212.5	2.7 ± 0.2	1.4	-	0.5	[92]
UTIO-nanowhiskers	-	2×20	6.13	11.15	1.4	[93]
C-ESION120	7.9	4.2	11.9	22.9	1.5	[81]
ES-MION3	-	3.6	8.8	22.7	1.5	[94]
Ultrasmall Fe_3O_4	-	1.9	1.41	2.87	7	[95]
Fe_2O_3 -water	8 ± 2	4.9 ± 0.6	17.6	35.8	1.5	[96]
Fe_2O_3 -Citrate	18 ± 4	5 ± 1	14.5	66.9	1.5	[96]
Fe_3O_4 -PMAA-PTTM	-	4.34 ± 1.54	24.2	67.2	0.5	[77]
Fe_3O_4 -PEG1100	10–15	4	7.3	17.5	1.4	[97]
PEG750-VSION	19.8	3.5 ± 0.6	1.74	40.6	9.4	[98]
PEG2000-VSION	22.2	3.5 ± 0.6	1.12	31.1	9.4	[98]
Ultrasmall Fe_3O_4	5.8	1.7	8.20	16.67	1.4	[79]
Ultrasmall Fe_3O_4	5.8	2.2	6.15	28.62	1.4	[79]
Metal-Doped IONPs						
Cu4-NP	16.1	3.5	15.7	32.8	1.5	[99]
EuIO-14 nanocubes	14.0 ± 1.9	14.0 ± 1.9	36.79 ± 1.16	97.52 ± 2.16	0.5	[100]
ZnFe_2O_4	-	4	7.93	14.64	1.5	[101]
NiFe_2O_4	-	5	6.85	12.92	1.5	[101]
$\text{Zn}_{0.3}\text{Fe}_{2.7}\text{O}_4/\text{SiO}_2$	-	18	615	1657	0.13×10^{-3}	[102]

4.2. Synthesis

Co-precipitation and thermal decomposition are the most frequently used methods to produce iron oxide nanoparticles. In addition, the extensive work on iron oxide nanoparticles over the last decade is bringing new procedures every year for the synthesis of nanoparticles of different sizes, shapes and composition and, hence, magnetic behaviour. In this section, the most remarkable methods are briefly described pointing out those which render nanoparticles with positive contrast capabilities.

4.2.1. Co-Precipitation

The co-precipitation protocol is the most used throughout the literature. It is based on the precipitation of iron oxides throughout a mixture of aqueous solutions of ferrous and ferric salts at a 2:1 ratio under basic conditions. The success of the co-precipitation method lies in its simplicity, flexibility and the hydrophilicity of the nanoparticles. However, it also shows some associated drawbacks such as the lack of control over the uniformity of the nanoparticles [103]. Modifications in the co-precipitation protocol can render ultrasmall iron oxide nanoparticles (USPIO) for T_1 -MRI. A high increase in the temperature of the reaction, combined with different polymers, has been used to develop nanoparticles between 3 and 8 nm with associated longitudinal relaxivities of up to $9 \text{ mM}^{-1} \text{ s}^{-1}$ at 4.7 T and $31 \text{ mM}^{-1} \text{ s}^{-1}$ at 1 T [90,104].

4.2.2. Thermal Decomposition

This well-known method, based on the decomposition of organic precursors at very high temperatures, has been widely utilised because of the high uniformity, crystallinity and control over the size of the nanoparticles. These nanoparticles are hydrophobic and therefore only stable in hydrophobic solvents, which implies an extra reaction step to stabilise the nanoparticles in physiological media. Despite this inconvenience, the control over the hydrodynamic size allows the obtention of USPIO with potential in positive contrast [87]. Wei et al. described the thermal decomposition of Fe(oleate)_3 in the presence of 1-tetradecene, 1-hexadecene and 1-octadecene, rendering nanoparticles from 2.5 to 7.0 nm of a maghemite core oxidised with trimethylamine N-oxide. The nanoparticles, stabilised in water using a ligand exchange reaction with a zwitterionic dopamine sulfonate (ZDS), showed a modest $r_1 = 5.2 \text{ mM}^{-1} \text{ s}^{-1}$ at 1.5 T and $1.5 \text{ mM}^{-1} \text{ s}^{-1}$ at 7 T [78]. Another remarkable example describes the synthesis of USPIO by decomposition of Fe(acac)_3 at 300 °C in the presence of oleic acid, oleylamine, hexadecanediol and oleyl alcohol as solvent. Ligand exchange with different bisphosphonate-based ligands provided nanoparticles with a magnetic core of 3.6 nm and a maximum $r_1 = 11 \text{ mM}^{-1} \text{ s}^{-1}$ at 1.5 T [98].

4.2.3. Polyol Synthesis

Polyol synthesis has been gaining attention in the recent years for the synthesis of IONPs. This method allows for an easy scaling-up of the reaction in a single-step reaction producing hydrophilic nanoparticles, although aggregation often happens. The method essentially consists of the reduction of the organometallic precursor in the presence of different polyols such as trimethylene glycol, propylene glycol or ethylene glycol. The role of the polyol has been reported not only as stabiliser but also as reducing agent [105].

Concerning IONPs with T_1 capabilities, the reduction of Fe(acac)_3 in diethylene glycol at 200 °C, under an inert atmosphere provided nanoparticles with 8 nm of hydrodynamic size and 3 nm of core size. These small particles exhibited $r_1 = 12 \text{ mM}^{-1} \text{ s}^{-1}$ at 1.41 T with a low $r_2/r_1 = 2.4$ [106]. Another reported example depicts a one-pot reaction of 5.4 nm IONPs by reduction of Fe(acac)_3 in the presence of triethylene glycol and HOOC-PEG-COOH at 260 °C. Under these conditions, the synthesised particles showed a $r_1 = 19.7 \text{ mM}^{-1} \text{ s}^{-1}$ at 1.5 T with a r_2/r_1 ratio of 2.0 [84].

4.2.4. Microwave Assisted Synthesis

Due to the simplicity, fast kinetics and reproducibility of the reactions, microwave-assisted synthesis of IONPs has grown lately. The use of microwaves ensures a very fast and homogeneous heating in the sample, which translates in a narrow size distribution of the nanoparticles [107]. Regarding the synthesis of IONPs for T_1 contrast, our group has been deeply involved in the use of microwaves. Essentially, extremely small iron oxide cores (~ 2.5 nm) can be achieved with FeCl_3 as iron source. The reaction is conducted at 100°C for 10 min in the presence of hydrazine hydrate (reducing agent) and a surfactant, usually dextran or sodium citrate. In a first approach, a $r_1 = 5.97 \text{ mM}^{-1} \text{ s}^{-1}$ at 1.5 T was obtained using (FITC)-dextran or dextran 6KDa as surfactant [108,109]. After these first approaches, better longitudinal relaxivities were observed using sodium citrate as surfactant. In this case, an increase in the temperature of the reaction turns over the contrast capabilities from T_2 to T_1 with an $r_1 = 11.9 \text{ mM}^{-1} \text{ s}^{-1}$ at 1.5 T when the reaction is performed at 120°C [81]. Very recently, Fernandez-Barahona et al. increased this value up to $15.7 \text{ mM}^{-1} \text{ s}^{-1}$, doping the iron oxide core with 4% mol of Cu [99].

5. In Vivo Applications

The use of iron oxide nanoparticles as contrast agents for MRI has usually been associated with T_2 -MRI. This is one of the main reasons why the use of iron oxide-based contrast agents for MRI is far from standard in clinical practice. The dark (T_2) signal makes them difficult to distinguish from naturally occurring hypointense areas in many diseases—caused by calcium deposits, bleeding, other metals or any signal void present in the area of interest. Given this, the need for nontoxic positive contrast agents has led to intense research in the development of iron oxide nanoparticles that produce high T_1 -weighted MRI signals, becoming therefore, a very active topic.

5.1. Iron-Based and Iron Oxide Nanoparticles

In recent years, several research groups have been developing new iron-based probes, mostly for T_1 -MRI but also for dual contrast MRI. Regarding T_1 -MRI, some researchers have been able to show, *in vivo*, a positive contrast effect. In 2013 Ju et al. [110] elaborated non-toxic synthetic melanin-like nanoparticles complexed with paramagnetic Fe^{3+} ions and stabilised with PEG (PEGylated Fe^{3+} -MeINPs), which were inspired by the MRI signal-enhancing capability of natural melanin. These nanoparticles showed relaxivity values of $r_1 = 17 \text{ mM}^{-1} \text{ s}^{-1}$ and $r_2 = 18 \text{ mM}^{-1} \text{ s}^{-1}$ at 3 T, which are higher than those of existing T_1 -MRI contrast agents based on gadolinium (Gd) or manganese (Mn). *In vivo*, PEGylated Fe^{3+} -MeINPs showed a positive signal enhancement in the spleen and liver of healthy mice within 0.5 and 1.5 h, respectively, after intravenous injection. During the same year, Peng et al. [111] synthesised antiferromagnetic α -iron oxide-hydroxide (α -FeOOH) nanocolloids, with diameters of 2–3 nm, which were placed inside the mesopores of worm-like silica nanoparticles. These nanocomposites exhibited a low r_2/r_1 ratio of 1.9, making them suitable as T_1 -weighted contrast agents. The *in vivo* experiments carried out showed a positive enhancement in the brain, bladder and kidneys of healthy mice. Moreover, in 2015, Iqbal et al. [85] produced biocompatible silica-coated superparamagnetic IONPs with diameters of ~ 4 nm, which showed *in vivo* T_1 contrast enhancement in the heart, liver, kidney and bladder of healthy mice. In addition, Macher et al. [93] developed an innovative T_1 MRI contrast agent, ultrathin iron oxide nanowhiskers. These nanostructures, with dimensions of 2×20 nm, possessed a high surface-to-volume ratio, leading to a strong paramagnetic signal, a property suitable for T_1 contrast. *In vivo* experiments showed a positive contrast enhancement in rat models after intraperitoneal (IP) and subcutaneous injection of the nanowhiskers. In 2019, Tao et al. [77] synthesised (poly(acrylic acid)-poly(methacrylic acid) iron oxide nanoparticles (PMAA-PTTM-IONPs) 4.34 nm in diameter with a low r_2/r_1 ratio of 2.78, adequate for T_1 -weighted contrast agents. *In vivo* experiments in mouse models showed biocompatibility and T_1 contrast enhancement in liver and kidney.

Even though the previously described probes were shown to provide contrast enhancement during in vivo T_1 -MRI, no specific in vivo application was described for them; thus, only their biodistribution was tested. Nevertheless, different research groups have developed probes for particular applications such as magnetic resonance angiography (MRA) and tumour imaging.

MRA has been shown to be a very helpful technique in clinical imaging. With its use, several diseases could be detected including myocardial infarction, renal failure, atherosclerotic plaque, thrombosis and tumour angiogenesis. Regarding research carried out on MRA, in 2011 Kim et al. [87] synthesised ultrasmall iron oxide nanoparticles (ESION, size < 4 nm) capped using poly(ethylene glycol)-derivatised phosphine oxide (PO-PEG) ligands, which enabled clear observation of various blood vessels, with sizes down to 0.2 mm, during in vivo T_1 -MRI in rat models. They were able to maintain the bright signal of blood vessels for 1 h on dynamic time-resolved MR angiography, showing that this type of probe can be used for T_1 enhanced blood pool MRI (Figure 2).

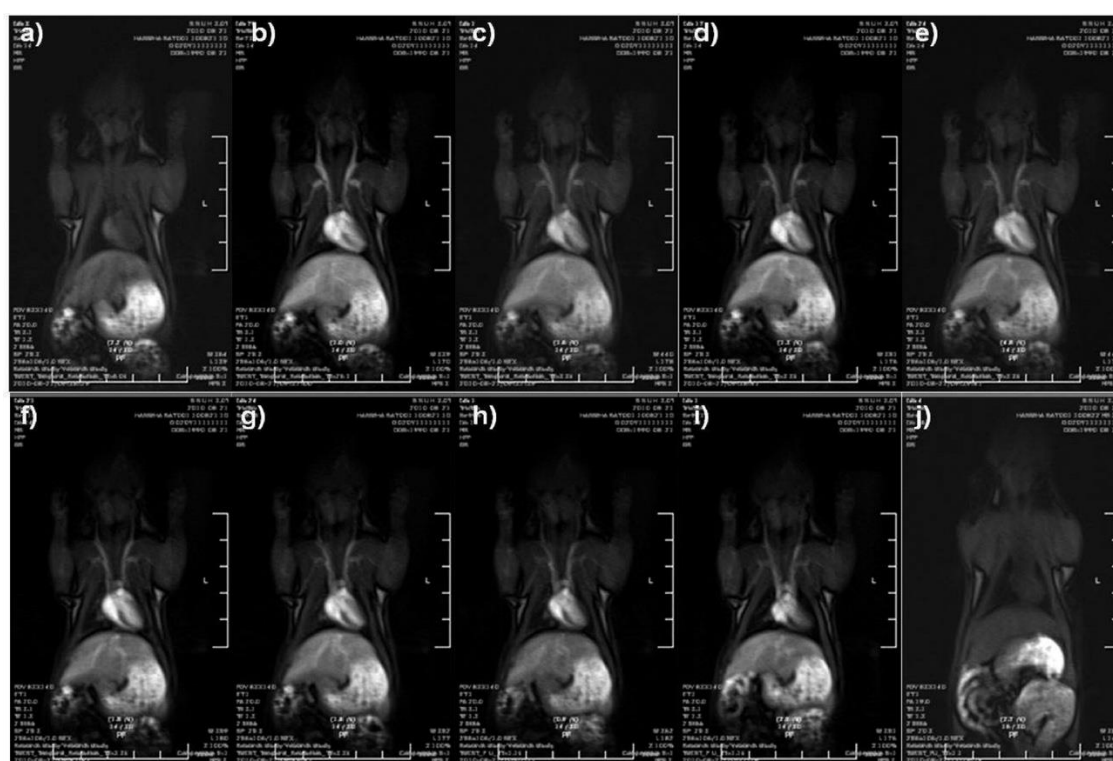


Figure 2. ESION-enhanced in vivo MR images with dynamic time-resolved MR sequence acquired at (a) 0 s (b) 30 s, (c) 1 min, (d) 2 min, (e) 3 min, (f) 5 min, (g) 10 min, (h) 30 min, (i) 60 min, and (j) 1 day after the injection. Reproduced with permission from [87], published by ACS, 2011.

Furthermore, in 2014 Chan et al. [83] produced multidentate block-copolymer-stabilised ultrasmall superparamagnetic iron oxide nanoparticles (MDBC-USPIOs), with diameters <5 nm and a r_2/r_1 ratio of 4.74 to test them as a promising T_1 -positive contrast agent for in vivo MRI. Results from in vivo MRI showed a strong blood signal enhancement after their intravenous injection in mouse models. During the same year, Liu et al. [91] developed glutathione-coated iron oxide nanoparticles (GSH-IONPs) with sizes of around 3.75 nm and a r_2/r_1 ratio of 2.28 as a novel T_1 -MRI contrast agent. The in vivo results showed a strong vascular enhancement at the carotid artery and superior sagittal sinus of healthy mice models, making it a promising contrast agent for thrombus detection.

In 2015, Bhavesh et al. [108] proposed an extremely fast microwave synthesis of fluorescein-labelled dextran-coated extremely small IONPs for their use as a contrast agent for T_1 -weighted MRI. This method yielded very small NPs with hydrodynamic diameters of 21.5 nm and with a r_2/r_1 ratio of 4.7 suitable for T_1 -MRI. In vivo MRA of healthy mice showed a clear depiction of the main vascular

architecture; furthermore, high quality visualisation of small vessels was maintained even 90 min post NP injection, highlighting the advantage of these NPs to be used as a contrast agent for blood pool imaging applications. In 2017, Pellico et al. [81] described the changes produced on the relaxometric properties of IONPs when the thickness of their organic coating is modified. For that purpose, this group synthesised all IONPs using a microwave-driven synthesis method; however, in order to change the coating layer thickness, different syntheses were carried out heating at different temperatures. Results showed that IONPs with a thinner coating yielded an excellent positive T_1 -MRI contrast, more specifically NPs synthesised at 120 °C. These NPs, with a hydrodynamic size of 7.9 nm and a r_2/r_1 ratio of 1.9 showed great contrast enhancement in both body and brain MRA of healthy mice, providing the possibility of better visualising their vasculature. In 2018, Vangijzegem et al. [98] synthesised very small PEGylated iron oxide nanoparticles (VSIONPs) with core sizes of 3.5 nm that showed positive contrast in in vivo MRA, enabling the heart chamber and the vena cava of healthy mice to be observed.

Regarding research on T_1 -weighted MR tumour imaging, in 2014 Wu et al. [112] produced mesoporous silica NPs with drug-labelled USPIOs confined within the mesoporous matrix (Fe-MSNs) as a pH-responsive theranostic platform. The tumour accumulation, driven by the enhanced permeability and retention effect (EPR), was confirmed by the T_1 enhancement in the affected site. Moreover, the unique metal–ligand coordination bonding between Fe species and the anticancer drug molecules provided the carrier with a pH-responsive drug release feature, triggering a controlled drug release under the acidic microenvironment in the tumour area. Moreover, Shen et al. [94] in 2017 synthesised extremely small 3.6 nm magnetic iron oxide nanoparticles (ES-MIONs) functionalised with dimeric RGD peptide (RGD₂) and PEG methyl ether (mPEG), which were afterwards loaded with the anticancer drug doxorubicin hydrochloride (DOX), as a tumour targeting theranostic platform. In this probe, the ES-MIONs serve as the contrast agent for T_1 -MRI, while RGD₂ is used for tumour targeting and DOX for chemotherapy. In vivo experiments on tumour-bearing mice showed an enhanced T_1 -MRI signal when using this platform together with partial regression of tumours due to active targeting and chemotherapy. Furthermore, Li et al. [88] in 2019 developed dynamically reversible iron oxide nanoparticle assemblies (IONAs) consisting of ES-IONs cross-linked by small molecular aldehyde derivative ligands. The linkage of these ligands is cleaved in the presence of acidic environments, such as tumours, releasing ES-IONs that are capable of producing contrast in T_1 -weighted MRI (Figure 3a). To demonstrate the specificity of the tandem linkage-cleavage, pH-insensitive cross-linked iron oxide nanoparticles (Ins-IONAs) and micelle-like pH sensitive polymer-assisted iron oxide nanoparticle assemblies (PIONAs) of similar sizes were used as controls (Figure 3a). In vivo experiments on tumour-bearing mice clearly indicated that the IONAs could amplify the T_1 -MRI signal, whilst Ins-IONAs and PIONAs showed significantly lower intensities (Figure 3b).

In addition to the undertaken research to find new probes that serve as contrast agents for T_1 -weighted MRI, there have been some research groups that have focused on developing probes for dual contrast MRI, that is, probes that are capable of producing both negative (T_2) and positive (T_1) contrast. In MRI, T_1 -weighted images typically provide better spatial resolution, while T_2 -weighted images can provide enhanced detection of lesions. For this reason, dual contrast probes could potentially provide better imaging information leading to higher diagnostic accuracy. Regarding research in this field, Jung et al. [86] in 2014 synthesised 5 nm SPIONs that, as shown using in vivo MRA experiments in rat models, were capable of producing both positive and negative contrast in MRA by using different acquisition pulses. On the one hand, ultrashort echo (UTE) sequence, which differently to the sequences explained in Section 2 use a radial sampling of the k-space to minimise T_E , positively enhanced vascular signals in MR angiography, providing highly resolved vessel structures. In addition, typical gradient sequences such as fast low angle shot (FLASH) acquisition yielded strong negative vessel contrast, resulting in a higher number of discernible vessel branches. Moreover, in 2018 Alipour et al. [82] developed 11 nm silica coated cubic SPIONs as a dual-mode contrast agent for T_1 and T_2 MRI. In vivo investigations on a 3 T MRI scanner demonstrated both positive and negative contrast enhancement 70 min post intravenous injection in healthy rat models.

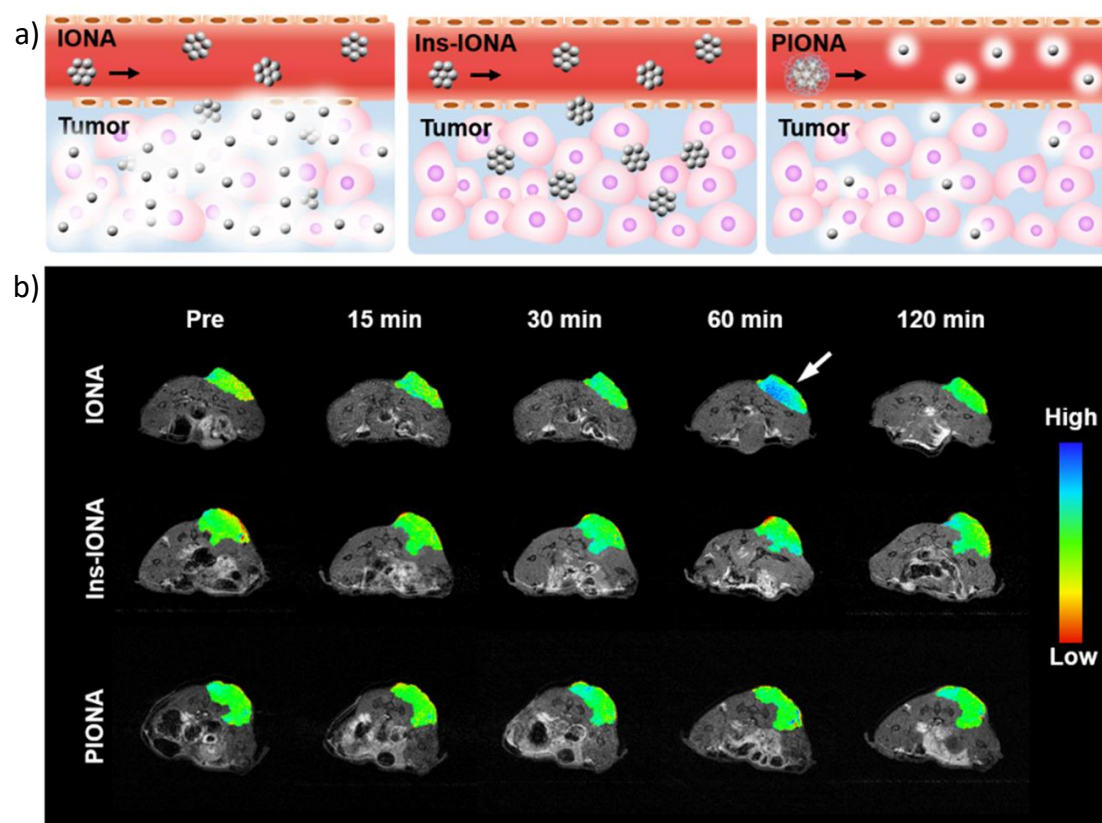


Figure 3. (a) Schematic illustration of the structural changes of iron oxide nanoparticle assemblies (IONAs), Ins-IONAs and polymer-assisted IONAs (PIONAs) in blood flow. The IONAs and Ins-IONAs are stable in blood circulation. After accumulation in tumour, IONAs further disassemble into dispersed ESIONs for non-linear amplification of MR imaging, while Ins-IONAs remain in the quenched T_1 MR state. PIONAs gradually dissociate during the blood circulation even before their accumulation in tumour. (b) T_1 -weighted MR images of tumour-bearing mice before and after i.v. injection of IONAs, Ins-IONAs and PIONAs. Modified and reproduced with permission from [88], published by ACS, 2019.

5.2. Doped Iron Oxide Nanoparticles

Throughout the past years, some metals have been integrated into IONPs in order to get better T_1 enhancement. Among different metals, focus remains on gadolinium (Gd), which are not included since our goal is focusing on alternatives, and manganese (Mn); however, there are some studies that use other metals such as copper (Cu) and europium (Eu).

Manganese-based contrast agents, similarly to Gd contrast agents, can significantly enhance the positive contrast in T_1 -weighted MRI. Furthermore, they can serve as contrast agents for visualising sub-anatomic structures and activities of brain and heart by taking advantage of Mn^{2+} as a biological calcium analogue. Nevertheless, their high toxicity limits their clinical applications, and for that reason, it is highly desirable to develop alternative non-toxic manganese contrast agents for clinical MRI. Several research groups have been recently developing manganese-containing iron oxide nanoparticles as alternative positive MRI contrast agents. In 2013, Li et al. [113] synthesised nontoxic ultrasmall manganese ferrite ($MnFe_2O_4$) nanoparticles of 2–3 nm that were shown to enhance the T_1 contrast in the liver, kidneys and brain of healthy mice during in vivo MRI. Similarly, in 2014 Huang et al. [114] produced Mn-doped IONPs of around 5 nm in diameter capable of functioning as a contrast agent for T_1 -weighted MRI having a low r_2/r_1 ratio of 2.6. Post injection, in vivo T_1 -MRI showed a brighter signal in the liver regions of healthy mice. Furthermore, in 2015 Zhang et al. [115] synthesised bovine serum albumin-coated manganese-doped IONPs (MnIO-BSA), 5 nm in size and with a low r_2/r_1 ratio of 2.18, as a theranostic platform for tumour targeting. The probe, once accumulated in the tumour,

was able to provide contrast in T_1 -weighted MRI and be heated using an external NIR light source for photothermal therapy (PTT) purposes. The in vivo MRI experiments using a tumour-bearing mouse model exhibited significant signal enhancement (about two times) at the tumour site. Furthermore, it was demonstrated that hyperthermia caused by the photothermal effect of the MnIO-BSA nanoparticles under NIR laser irradiation resulted in significant death of the cancer cells.

Only a few studies use copper or europium as doping metals. In 2019, our group synthesised extremely small citrate-coated iron oxide nanoparticles doped with Cu as a T_1 -weighted contrast agent [99]. After studying several Cu doping amounts, IONPs doped with 4% mol of Cu (Cu4-NPs) were chosen as the best probe. Cu4-NPs presented a hydrodynamic diameter of ~ 15 nm and a core size of ~ 3.5 nm. Moreover, they showed a high r_1 value of $15.7 \text{ mM}^{-1} \text{ s}^{-1}$ at 1.5 T and a low r_2/r_1 ratio of 2.1. Interestingly, the reason for this increase in the r_1 values was due to the distribution of Cu atoms within the iron oxide structure. In vivo MRA showed that Cu4-NPs provided high-quality images with fine details of the vasculature up to 30 min post injection (Figure 4). In order to explore a different probe application, RGD molecules were conjugated to the surfaces of Cu4-NPs for active tumour targeting. In vivo T_1 -MRI experiments on tumour-bearing mice showed an increased positive signal on the tumour after intravenous injection of the RGD-Cu4-NP, further confirming their use as a positive contrast agent. Europium was used by Yang et al. [100] in 2015; this group produced citrate-coated europium-doped iron oxide nanocubes, 14 nm in size, with high r_1 values of $36.8 \text{ mM}^{-1} \text{ s}^{-1}$ at 0.5 T and a low r_2/r_1 ratio of 2.65 for T_1 -weighted MRI. In vivo results showed an increase in signal brightness in the heart of healthy mice.

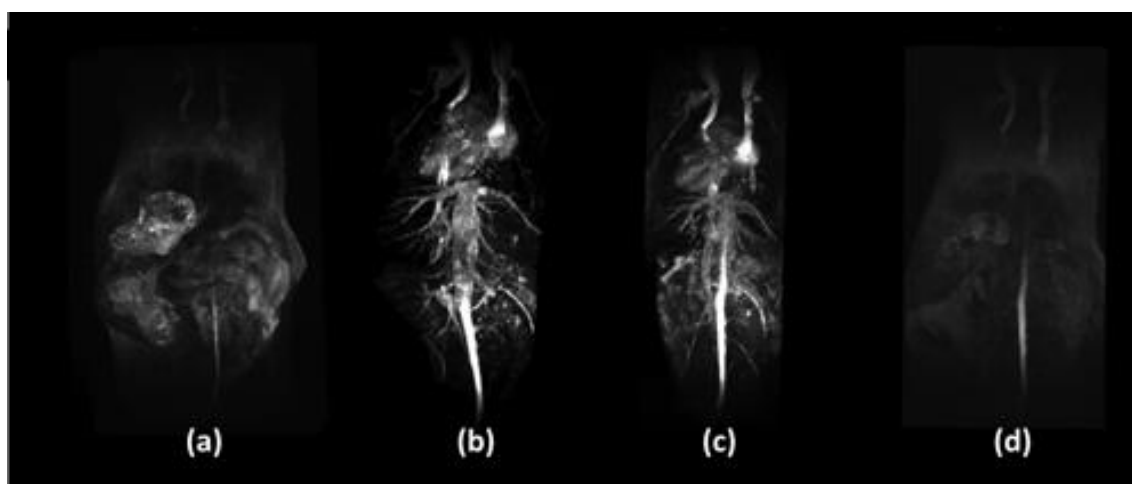


Figure 4. MRI (T_1 -weighted imaging) body angiography in healthy mice, before (a) and after the intravenous injection, $0.04 \text{ mmol Fe kg}^{-1}$, of Cu4-NPs at (b) 15 min (c) 30 min (d) 45 min. Reproduced with permission from [99].

5.3. Multimodal T_1 -Iron Oxide Nanoparticles

The combination of MRI with complementary imaging techniques such as PET or SPECT (Single Photon Emission Computed Tomography), allows protocols to be developed that exploit their synergy. Although a great number of multimodal IONPs have been described for T_2 -weighted MRI, only a few examples have been reported for IONPs acting as positive contrast agents [116].

These examples are focused on the combination of biocompatible iron oxide nanoparticles with radionuclides, such as Gallium-68 (^{68}Ga) or Technetium-99m ($^{99\text{m}}\text{Tc}$) for PET and SPECT, respectively.

^{68}Ga has been successfully used with IONPs in several multimodal experiments. In 2016, Pellico et al. developed a T_1 -weighted MRI/PET platform consisting of extremely small ^{68}Ga -doped IONPs synthesised using a microwave-driven protocol, which were diversely functionalised for their use in several applications. For example, ^{68}Ga core-doped IONPs functionalised with RGD

were synthesised for tumour angiogenesis targeting. This probe presented a hydrodynamic size of 20.6 nm with core sizes of 2.5 nm. Furthermore, it showed a r_1 value of $5.7 \text{ mM}^{-1} \text{ s}^{-1}$ at 1.5 T and a low r_2/r_1 ratio of 3.9, making it suitable for T_1 -weighted MRI. In vivo MRI experiments in tumour-bearing mouse models showed a brighter signal in the tumour 24 h post NP injection.¹¹⁴ In addition, in 2018 the group synthesised a biorthogonal nano-radiotracer for in vivo pretargeted molecular imaging of atherosclerosis. This probe was based on the in vivo tetrazine ligation of an imaging and a targeting moiety, which were functionalised with a tetrazine (Tz) and a trans-cyclooctene (TCO), respectively. The imaging part consisted of ^{68}Ga -doped IONPs that provided simultaneous PET and T_1 -MRI signals, while the atherosclerosis targeting part consisted of an oxidised LDL (Low-Density Lipoprotein)-targeting IgM antibody (E-06). ^{68}Ga -IONP-Tz presented a hydrodynamic diameter of 15.5 nm with a core size of 2.8 nm. Moreover, they showed a high r_1 value of $7.1 \text{ mM}^{-1} \text{ s}^{-1}$ at 1.5 T and a low r_2/r_1 ratio of 2.5, making them useful as contrast agents for T_1 -weighted MRI. Ex vivo T_1 -MRI of the aorta of an atherosclerotic mouse model showed a brighter signal on the atherosclerotic plaque [117].

Regarding research carried out on $^{99\text{m}}\text{Tc}$ -doped IONPs, in 2013 Sandiford et al. [118] produced PEGylated bisphosphonate-coated USPIOs to use as a multimodal platform in T_1 -MRI and SPECT. This probe showed a high r_1 value of $9.5 \text{ mM}^{-1} \text{ s}^{-1}$ at 3 T and a low r_2/r_1 ratio of 2.9, enabling their use as positive contrast agents. In vivo MRI experiments in healthy BALB/C mice showed a strong T_1 effect post NP injection resulting in a substantial increase in the signal from blood, making vessels, the heart compartments and other highly vascularised organs such as the spleen visible (Figure 5a). This biodistribution was also observed using SPECT/CT with the nanoparticles circulating 40 min after i.v. injection (Figure 5b).

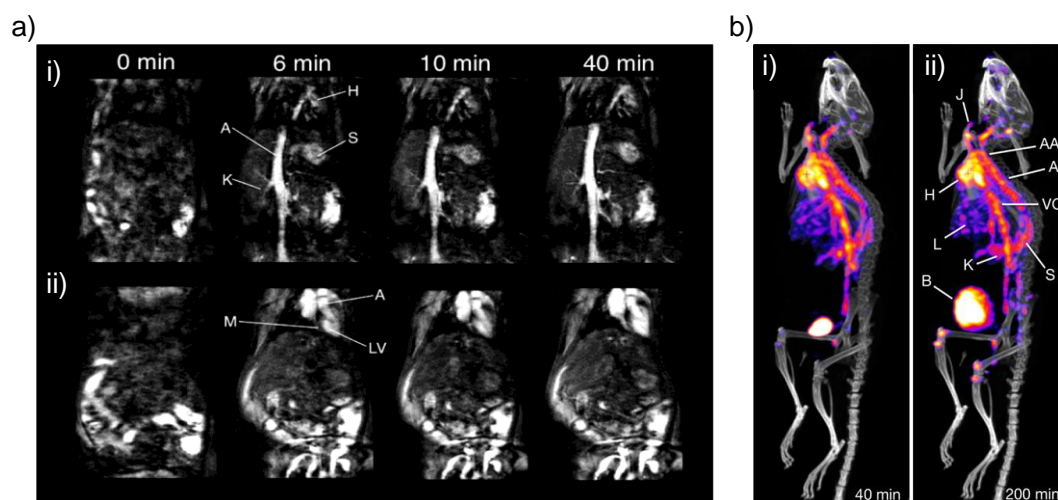


Figure 5. (a) In vivo MRI studies with PEG(5)-BP-USPIO: T_1 -weighted images showing the increase in signal from blood in the vessels and the heart (ii) at different time points ($t = 0 \text{ min}$, pre-injection). (b) Maximum intensity projection SPECT-CT images after i.v. injection of radiolabelled ($^{99\text{m}}\text{Tc}$) PEG(5)-BP-USPIO at the first (i, 40 min) and last (ii, 200 min) time points. Labels: H = heart, S = spleen, K = kidney, A = aorta, M = myocardium, LV = left ventricle, J = jugular vein, AA = aortic arch, VC = vena cava, L = liver, B = bladder. Modified and reproduced with permission from [118].

Besides the use of T_1 -IONPs for dual MRI(T_1)/PET or SPECT imaging, G. Wang et al. reported an example for MRI(T_1)/CT imaging. In this case, ultrasmall magnetite nanoparticles were combined with Au nanocages rendering F-AuNC@ Fe_3O_4 . The ultrasmall Fe_3O_4 particles (2.2 nm) showed a $r_1 = 6.3 \text{ mM}^{-1} \text{ s}^{-1}$, providing a T_1 -enhancement in MRI, whilst a strong X-ray attenuation was observed due to the AuNC [119].

6. Conclusions and Future Perspectives

In the last decade, significant effort has been made in the design of iron oxide formulations for T_1 contrast due to the associated toxicity in the application of the traditional Gd^{3+} contrast agents. We have summarised the most important features to optimise IONPs as a T_1 contrast agent, i.e., ultrasmall core size with moderate crystallinity (usually maghemite ($\gamma\text{-Fe}_2\text{O}_3$)) and high colloidal stability with hydrodynamic sizes ranging from 5 to 20 nm. With the focus on the physicochemical characteristics of T_1 -IONPs such as iron phase, core size, type of coating or the surface charge, there is still room for improvement using the described synthetic procedures or novel strategies. Although the optimisation of these properties brings associated higher T_1 performance, the longitudinal relaxivities are still far from those obtained in some Gd^{3+} -based nanoparticles such as gadofullerens, gadolinium oxide particles, Gd-nanocages or Gd^{3+} conjugated to mesoporous silica nanoparticles [120]. It is noteworthy that the application of Gd^{3+} -based agents has been thoroughly studied for many years, whilst the potential of IONPs as T_1 agents is an emerging field of research. Therefore, there is still a lack of consensus to determine the best scenario for T_1 -IONPs. To date, the variability of the particles showing different physicochemical properties and MRI responses is high. However, a broad number of applications have been reported including not only MRI but also multimodal imaging for molecular imaging applications or metal-doped particles for therapeutic purposes. In addition, other issues such as biocompatibility, pharmacokinetics or delivery pathways must be studied in advance to guarantee their clinical translation. In conclusion, there is great potential in the development of T_1 -IONPs with several concerns to be evaluated in detail. Further studies must bring a clear conclusion about the best properties and then adapt the formulations to clinical requirements.

Funding: F.H. was funded through the Spanish Ministry for Economy and Competitiveness (MEyC), grant number [SAF2016-79593-P] and the Ministry of Science, grant number [RED2018-102469-T]. J.R.-C. was funded through the Spanish Ministry for Economy and Competitiveness (MEyC), grant number [SAF2017-84494-C2-R], and the Gobierno Vasco, Dpto. Industria, Innovación, Comercio y Turismo under the ELKARTEK Program (Grant No. KK-2019/bmG19). CIC biomaGUNE is supported by the Maria de Maeztu Units of Excellence Program from the Spanish State Research Agency—Grant No. MDM-2017-0720.

Conflicts of Interest: The authors declare no conflict of interest.

References

- Markl, M.; Leupold, J. Gradient echo imaging. *J. Magn. Reson. Imaging* **2012**, *35*, 1274–1289. [[CrossRef](#)] [[PubMed](#)]
- Lohrke, J.; Frenzel, T.; Endrikat, J.; Alves, F.C.; Grist, T.M.; Law, M.; Lee, J.M.; Leiner, T.; Li, K.-C.; Nikolaou, K.; et al. 25 Years of Contrast-Enhanced MRI: Developments, Current Challenges and Future Perspectives. *Adv. Ther.* **2016**, *33*, 1–28. [[CrossRef](#)] [[PubMed](#)]
- Na, H.B.; Hyeon, T. Nanostructured T_1 MRI contrast agents. *J. Mater. Chem.* **2009**, *19*, 6267–6273. [[CrossRef](#)]
- Bridot, J.-L.; Faure, A.-C.; Laurent, S.; Riviere, C.; Billotey, C.; Hiba, B.; Janier, M.; Josseland, V.; Coll, J.-L.; Elst, L.V.; et al. Hybrid Gadolinium Oxide Nanoparticles: Multimodal Contrast Agents for in Vivo Imaging. *J. Am. Chem. Soc.* **2007**, *129*, 5076–5084. [[CrossRef](#)] [[PubMed](#)]
- Park, J.Y.; Baek, M.J.; Choi, E.S.; Woo, S.; Kim, J.H.; Kim, T.J.; Jung, J.C.; Chae, K.S.; Chang, Y.; Lee, G.H. Paramagnetic Ultrasmall Gadolinium Oxide Nanoparticles as Advanced T_1 MRI Contrast Agent: Account for Large Longitudinal Relaxivity, Optimal Particle Diameter, and In Vivo T_1 MR Images. *ACS Nano* **2009**, *3*, 3663–3669. [[CrossRef](#)]
- Evanics, F.; Diamante, P.R.; van Veggel, F.C.J.M.; Stanisiz, G.J.; Prosser, R.S. Water-Soluble GdF_3 and GdF_3/LaF_3 Nanoparticles Physical Characterization and NMR Relaxation Properties. *Chem. Mater.* **2006**, *18*, 2499–2505. [[CrossRef](#)]
- Cheung, E.N.M.; Alvares, R.D.; Oakden, W.; Chaudhary, R.; Hill, M.L.; Pichaandi, J.; Mo, G.C.H.; Yip, C.; Macdonald, P.M.; Stanisiz, G.J.; et al. Polymer-Stabilized Lanthanide Fluoride Nanoparticle Aggregates as Contrast Agents for Magnetic Resonance Imaging and Computed Tomography. *Chem. Mater.* **2010**, *22*, 4728–4739. [[CrossRef](#)]

8. Hifumi, H.; Yamaoka, S.; Tanimoto, A.; Citterio, D.; Suzuki, K. Gadolinium-Based Hybrid Nanoparticles as a Positive MR Contrast Agent. *J. Am. Chem. Soc.* **2006**, *128*, 15090–15091. [\[CrossRef\]](#)
9. Shen, Z.; Fan, W.; Yang, Z.; Liu, Y.; Bregadze, V.I.; Mandal, S.K.; Yung, B.C.; Lin, L.; Liu, T.; Tang, W.; et al. Exceedingly Small Gadolinium Oxide Nanoparticles with Remarkable Relaxivities for Magnetic Resonance Imaging of Tumors. *Small* **2019**, *15*, 1903422. [\[CrossRef\]](#)
10. Mortezaazadeh, T.; Gholibegloo, E.; Alam, N.R.; Dehghani, S.; Haghighi, S.; Ghanaati, H.; Khoobi, M. Gadolinium(III) oxide nanoparticles coated with folic acid-functionalized poly(β -cyclodextrin-co-pentetic acid) as a biocompatible targeted nano-contrast agent for cancer diagnostic: In vitro and in vivo studies. *Magn. Reson. Mater. Phys. Biol. Med.* **2019**, *32*, 487–500. [\[CrossRef\]](#)
11. Kumar, S.; Meena, V.K.; Hazari, P.P.; Sharma, S.K.; Sharma, R.K. Rose Bengal attached and dextran coated gadolinium oxide nanoparticles for potential diagnostic imaging applications. *Eur. J. Pharm. Sci.* **2018**, *117*, 362–370. [\[CrossRef\]](#) [\[PubMed\]](#)
12. Qiu, Q.; Wen, Y.; Dong, H.; Shen, A.; Zheng, X.; Li, Y.; Feng, F. A highly sensitive living probe derived from nanoparticle-remodeled neutrophils for precision tumor imaging diagnosis. *Biomater. Sci.* **2019**, *7*, 5211–5220. [\[CrossRef\]](#) [\[PubMed\]](#)
13. Cui, D.; Lu, X.; Yan, C.; Liu, X.; Hou, M.; Xia, Q.; Xu, Y.; Liu, R. Gastrin-releasing peptide receptor-targeted gadolinium oxide-based multifunctional nanoparticles for dual magnetic resonance/fluorescent molecular imaging of prostate cancer. *Int. J. Nanomed.* **2017**, *12*, 6787–6797. [\[CrossRef\]](#) [\[PubMed\]](#)
14. Mastrogiacomo, S.; Kownacka, A.E.; Dou, W.; Burke, B.P.; de Rosales, R.T.; Heerschap, A.; Jansen, J.A.; Archibald, S.J.; Walboomers, X.F. Bisphosphonate Functionalized Gadolinium Oxide Nanoparticles Allow Long-Term MRI/CT Multimodal Imaging of Calcium Phosphate Bone Cement. *Adv. Healthc. Mater.* **2018**, *7*, 1800202. [\[CrossRef\]](#) [\[PubMed\]](#)
15. Dai, Y.; Wu, C.; Wang, S.; Li, Q.; Zhang, M.; Li, J.; Xu, K. Comparative study on in vivo behavior of PEGylated gadolinium oxide nanoparticles and Magnevist as MRI contrast agent. *Nanomed. Nanotechnol. Biol. Med.* **2018**, *14*, 547–555. [\[CrossRef\]](#)
16. Jiang, Y.; Zheng, W. Cardiovascular toxicities upon manganese exposure. *Cardiovasc. Toxicol.* **2005**, *5*, 345–354. [\[CrossRef\]](#)
17. Sidoryk-Wegrzynowicz, M.; Aschner, M. Manganese toxicity in the central nervous system: The glutamine/glutamate- γ -aminobutyric acid cycle. *J. Intern. Med.* **2013**, *273*, 466–477. [\[CrossRef\]](#)
18. Wolf, G.; Baum, L. Cardiovascular toxicity and tissue proton T_1 response to manganese injection in the dog and rabbit. *Am. J. Roentgenol.* **1983**, *141*, 193–197. [\[CrossRef\]](#)
19. Chevallier, P.; Walter, A.; Garofalo, A.; Veksler, I.; Lagueux, J.; Begin-Colin, S.; Felder-Flesch, D.; Fortin, M.-A. Tailored biological retention and efficient clearance of pegylated ultra-small MnO nanoparticles as positive MRI contrast agents for molecular imaging. *J. Mater. Chem. B* **2014**, *2*, 1779–1790. [\[CrossRef\]](#)
20. Huang, H.; Yue, T.; Xu, Y.; Xu, K.; Xu, H.; Liu, S.; Yu, J.; Huang, J. PEGylation of MnO nanoparticles via catechol-Mn chelation to improving T_1 -weighted magnetic resonance imaging application. *J. Appl. Polym. Sci.* **2015**, *132*, 2–9. [\[CrossRef\]](#)
21. Wang, P.; Yang, J.; Zhou, B.; Hu, Y.; Xing, L.; Xu, F.; Shen, M.; Zhang, G.; Shi, X. Antifouling manganese oxide nanoparticles: Synthesis, characterization, and applications for enhanced MR imaging of tumors. *ACS Appl. Mater. Interfaces* **2017**, *9*, 47–53. [\[CrossRef\]](#) [\[PubMed\]](#)
22. Chen, N.; Shao, C.; Qu, Y.; Li, S.; Gu, W.; Zheng, T.; Ye, L.; Yu, C. Folic Acid-Conjugated MnO Nanoparticles as a T_1 Contrast Agent for Magnetic Resonance Imaging of Tiny Brain Gliomas. *ACS Appl. Mater. Interfaces* **2014**, *6*, 19850–19857. [\[CrossRef\]](#) [\[PubMed\]](#)
23. Gallo, J.; Alam, I.S.; Lavdas, I.; Wylezinska-Arridge, M.; Aboagye, E.O.; Long, N.J. RGD-targeted MnO nanoparticles as T_1 contrast agents for cancer imaging—the effect of PEG length in vivo. *J. Mater. Chem. B* **2014**, *2*, 868–876. [\[CrossRef\]](#)
24. Li, J.; Wu, C.; Hou, P.; Zhang, M.; Xu, K. One-pot preparation of hydrophilic manganese oxide nanoparticles as T_1 nano-contrast agent for molecular magnetic resonance imaging of renal carcinoma in vitro and in vivo. *Biosens. Bioelectron.* **2018**, *102*, 1–8. [\[CrossRef\]](#) [\[PubMed\]](#)
25. Li, B.; Gu, Z.; Kurniawan, N.; Chen, W.; Xu, Z.P. Manganese-Based Layered Double Hydroxide Nanoparticles as a T_1 -MRI Contrast Agent with Ultrasensitive pH Response and High Relaxivity. *Adv. Mater.* **2017**, *29*, 1700373. [\[CrossRef\]](#) [\[PubMed\]](#)

26. McDonagh, B.H.; Singh, G.; Hak, S.; Bandyopadhyay, S.; Augestad, I.L.; Peddis, D.; Sandvig, I.; Sandvig, A.; Glomm, W.R. L-DOPA-Coated Manganese Oxide Nanoparticles as Dual MRI Contrast Agents and Drug-Delivery Vehicles. *Small* **2016**, *12*, 301–306. [[CrossRef](#)] [[PubMed](#)]
27. Cheng, Y.; Zhang, S.; Kang, N.; Huang, J.; Lv, X.; Wen, K.; Ye, S.; Chen, Z.; Zhou, X.; Ren, L. Polydopamine-Coated Manganese Carbonate Nanoparticles for Amplified Magnetic Resonance Imaging-Guided Photothermal Therapy. *ACS Appl. Mater. Interfaces* **2017**, *9*, 19296–19306. [[CrossRef](#)]
28. Zhan, Y.; Shi, S.; Ehlerding, E.B.; Graves, S.A.; Goel, S.; Engle, J.W.; Liang, J.; Tian, J.; Cai, W. Radiolabeled, Antibody-Conjugated Manganese Oxide Nanoparticles for Tumor Vasculature Targeted Positron Emission Tomography and Magnetic Resonance Imaging. *ACS Appl. Mater. Interfaces* **2017**, *9*, 38304–38312. [[CrossRef](#)]
29. Zhan, Y.; Zhan, W.; Li, H.; Xu, X.; Cao, X.; Zhu, S.; Liang, J.; Chen, X. In vivo dual-modality fluorescence and magnetic resonance imaging-guided lymph node mapping with good biocompatibility manganese oxide nanoparticles. *Molecules* **2017**, *22*, 2208. [[CrossRef](#)]
30. McMahon, M.T.; Bulte, J.W.M. Two decades of dendrimers as versatile MRI agents: A tale with and without metals. *Wiley Interdiscip. Rev. Nanomed. Nanobiotechnol.* **2018**, *10*, e1496. [[CrossRef](#)]
31. Dias, A.P.; da Silva Santos, S.; da Silva, J.V.; Parise Filho, R.; Ferreira, E.I.; El Seoud, O.; Giarolla, J. Dendrimers in the context of nanomedicine. *Int. J. Pharm.* **2020**, *573*, 118814. [[CrossRef](#)] [[PubMed](#)]
32. Hu, J.; Hu, K.; Cheng, Y. Tailoring the dendrimer core for efficient gene delivery. *Acta Biomater.* **2016**, *35*, 1–11. [[CrossRef](#)] [[PubMed](#)]
33. Opina, A.C.; Wong, K.J.; Griffiths, G.L.; Turkbey, B.I.; Bernardo, M.; Nakajima, T.; Kobayashi, H.; Choyke, P.L.; Vasalati, O. Preparation and long-term biodistribution studies of a PAMAM dendrimer G5-Gd-BnDOTA conjugate for lymphatic imaging. *Nanomedicine* **2015**, *10*, 1423–1437. [[CrossRef](#)] [[PubMed](#)]
34. Swanson, S.D.; Kukowska-Latallo, J.F.; Patri, A.K.; Chen, C.; Ge, S.; Cao, Z.; Kotlyar, A.; East, A.T.; Baker, J.R. Targeted gadolinium-loaded dendrimer nanoparticles for tumor-specific magnetic resonance contrast enhancement. *Int. J. Nanomedicine* **2008**, *3*, 201–210.
35. Li, F.; Yan, H.; Wang, J.; Li, C.; Wu, J.; Wu, S.; Rao, S.; Gao, X.; Jin, Q. Non-invasively differentiating extent of liver fibrosis by visualizing hepatic integrin $\alpha v \beta 3$ expression with an MRI modality in mice. *Biomaterials* **2016**, *102*, 162–174. [[CrossRef](#)]
36. Alamdari, N.H.; Alaei-Beirami, M.; Shandiz, S.A.S.; Hejazi, H.; Rasouli, R.; Saffari, M.; Ebrahimi, S.E.S.; Assadi, A.; Ardestani, M.S. Gd³⁺-Asparagine-Anionic Linear Globular Dendrimer Second-Generation G2 Complexes: Novel Nanobiohybrid Theranostics. *Contrast Media Mol. Imaging* **2017**, *2017*, 3625729.
37. Wang, R.; Luo, Y.; Yang, S.; Lin, J.; Gao, D.; Zhao, Y.; Liu, J.; Shi, X.; Wang, X. Hyaluronic acid-modified manganese-chelated dendrimer-entrapped gold nanoparticles for the targeted CT/MR dual-mode imaging of hepatocellular carcinoma. *Sci. Rep.* **2016**, *6*, 33844. [[CrossRef](#)]
38. Nguyen, T.H.; Bryant, H.; Shapsa, A.; Street, H.; Mani, V.; Fayad, Z.A.; Frank, J.A.; Tsimikas, S.; Briley-Saebo, K.C. Manganese G8 dendrimers targeted to oxidation-specific epitopes: In vivo MR imaging of atherosclerosis. *J. Magn. Reson. Imaging* **2015**, *41*, 797–805. [[CrossRef](#)]
39. Fan, Y.; Zhang, J.; Shi, M.; Li, D.; Lu, C.; Cao, X.; Peng, C.; Mignani, S.; Majoral, J.-P.; Shi, X. Poly (amidoamine) Dendrimer-Coordinated Copper(II) Complexes as a Theranostic Nanoplatfor for the Radiotherapy-Enhanced Magnetic Resonance Imaging and Chemotherapy of Tumors and Tumor Metastasis. *Nano Lett.* **2019**, *19*, 1216–1226. [[CrossRef](#)]
40. Kim, S.M.; Im, G.H.; Lee, D.G.; Lee, J.H.; Lee, W.J.; Lee, I.S. Mn²⁺-doped silica nanoparticles for hepatocyte-targeted detection of liver cancer in T₁-weighted MRI. *Biomaterials* **2013**, *34*, 8941–8948. [[CrossRef](#)]
41. Li, X.; Zhao, W.; Liu, X.; Chen, K.; Zhu, S.; Shi, P.; Chen, Y.; Shi, J. Mesoporous manganese silicate coated silica nanoparticles as multi-stimuli-responsive T₁-MRI contrast agents and drug delivery carriers. *Acta Biomater.* **2016**, *30*, 378–387. [[CrossRef](#)] [[PubMed](#)]
42. Pellico, J.; Ellis, C.M.; Miller, J.; Davis, J.J. Water gated contrast switching with polymer-silica hybrid nanoparticles. *Chem. Commun.* **2019**, *55*, 8540–8543. [[CrossRef](#)] [[PubMed](#)]
43. Wartenberg, N.; Fries, P.; Raccurt, O.; Guillermo, A.; Imbert, D.; Mazzanti, M. A Gadolinium Complex Confined in Silica Nanoparticles as a Highly Efficient T₁/T₂ MRI Contrast Agent. *Chem. Eur. J.* **2013**, *19*, 6980–6983. [[CrossRef](#)] [[PubMed](#)]
44. Taylor, K.M.L.; Kim, J.S.; Rieter, W.J.; An, H.; Lin, W.; Lin, W. Mesoporous Silica Nanospheres as Highly Efficient MRI Contrast Agents. *J. Am. Chem. Soc.* **2008**, *130*, 2154–2155. [[CrossRef](#)]

45. Carniato, F.; Tei, L.; Botta, M. Gd-Based Mesoporous Silica Nanoparticles as MRI Probes. *Eur. J. Inorg. Chem.* **2018**, *2018*, 4936–4954. [\[CrossRef\]](#)
46. Davis, J.J.; Huang, W.-Y.; Davies, G.-L. Location-tuned relaxivity in Gd-doped mesoporous silica nanoparticles. *J. Mater. Chem.* **2012**, *22*, 22848–22850. [\[CrossRef\]](#)
47. Fossheim, S.L.; Fahlvik, A.K.; Klaveness, J.; Muller, R.N. Paramagnetic liposomes as MRI contrast agents: Influence of liposomal physicochemical properties on the in vitro relaxivity. *Magn. Reson. Imaging* **1999**, *17*, 83–89. [\[CrossRef\]](#)
48. Leclercq, F.; Cohen-Ohana, M.; Mignet, N.; Sbarbati, A.; Herscovici, J.; Scherman, D.; Byk, G. Design, Synthesis, and Evaluation of Gadolinium Cationic Lipids As Tools for Biodistribution Studies of Gene Delivery Complexes. *Bioconj. Chem.* **2003**, *14*, 112–119. [\[CrossRef\]](#)
49. Qiu, L.H.; Zhang, J.W.; Li, S.P.; Xie, C.; Yao, Z.W.; Feng, X.Y. Molecular imaging of angiogenesis to delineate the tumor margins in glioma rat model with endoglin-targeted paramagnetic liposomes using 3T MRI. *J. Magn. Reson. Imaging* **2015**, *41*, 1056–1064. [\[CrossRef\]](#)
50. Song, Y.; Li, W.; Meng, S.; Zhou, W.; Su, B.; Tang, L.; Zhao, Y.; Wu, X.; Yin, D.; Fan, M.; et al. Dual integrin $\alpha v \beta 3$ and NRP-1-Targeting Paramagnetic Liposome for Tumor Early Detection in Magnetic Resonance Imaging. *Nanoscale Res. Lett.* **2018**, *13*, 380. [\[CrossRef\]](#)
51. Ren, L.; Chen, S.; Li, H.; Zhang, Z.; Zhong, J.; Liu, M.; Zhou, X. MRI-guided liposomes for targeted tandem chemotherapy and therapeutic response prediction. *Acta Biomater.* **2016**, *35*, 260–268. [\[CrossRef\]](#)
52. Woodside, D.G.; Tanifum, E.A.; Ghaghada, K.B.; Biediger, R.J.; Caivano, A.R.; Starosolski, Z.A.; Khounlo, S.; Bhayana, S.; Abbasi, S.; Craft, J.W., Jr.; et al. Magnetic Resonance Imaging of Atherosclerotic Plaque at Clinically Relevant Field Strengths (1T) by Targeting the Integrin $\alpha 4 \beta 1$. *Sci. Rep.* **2018**, *8*, 3733. [\[CrossRef\]](#) [\[PubMed\]](#)
53. Rieter, W.J.; Kim, J.S.; Taylor, K.M.; An, H.; Lin, W.; Tarrant, T.; Lin, W. Hybrid Silica Nanoparticles for Multimodal Imaging. *Angew. Chem. Int. Ed.* **2007**, *46*, 3680–3682. [\[CrossRef\]](#) [\[PubMed\]](#)
54. Lechevallier, S.; Mauricot, R.; Gros-Dagnac, H.; Chevreux, S.; Lemerrier, G.; Phonesouk, E.; Golzio, M.; Verelst, M. Silica-Based Nanoparticles as Bifunctional and Bimodal Imaging Contrast Agents. *Chempluschem* **2017**, *82*, 770–777. [\[CrossRef\]](#) [\[PubMed\]](#)
55. Mignot, A.; Truillet, C.; Lux, F.; Sancey, L.; Louis, C.; Denat, F.; Boschetti, F.; Bocher, L.; Gloter, A.; Stéphan, O.; et al. A Top-Down Synthesis Route to Ultrasmall Multifunctional Gd-Based Silica Nanoparticles for Theranostic Applications. *Chem. Eur. J.* **2013**, *19*, 6122–6136. [\[CrossRef\]](#)
56. Gizzatov, A.; Hernández-Rivera, M.; Keshishian, V.; Mackeyev, Y.; Law, J.J.; Guven, A.; Sethi, R.; Qu, F.F.; Muthupillai, R.; da Graça Cabreira-Hansen, M.; et al. Surfactant-free Gd^{3+} -ion-containing carbon nanotube MRI contrast agents for stem cell labeling. *Nanoscale* **2015**, *7*, 12085–12091. [\[CrossRef\]](#)
57. Servant, A.; Jacobs, I.; Bussy, C.; Fabbro, C.; Da Ros, T.; Pach, E.; Ballesteros, B.; Prato, M.; Nicolay, K.; Kostarelos, K. Gadolinium-functionalised multi-walled carbon nanotubes as a T_1 contrast agent for MRI cell labelling and tracking. *Carbon* **2016**, *97*, 126–133. [\[CrossRef\]](#)
58. Moghaddam, S.E.; Hernández-Rivera, M.; Zaibaq, N.G.; Ajala, A.; da Graça Cabreira-Hansen, M.; Mowlazadeh-Haghighi, S.; Willerson, J.T.; Perin, E.C.; Muthupillai, R.; Wilson, L.J. A New High-Performance Gadonanotube-Polymer Hybrid Material for Stem Cell Labeling and Tracking by MRI. *Contrast Media Mol. Imaging* **2018**, *2018*, 2853736. [\[CrossRef\]](#)
59. Richard, C.; Doan, B.T.; Beloeil, J.C.; Bessodes, M.; Tóth, É.; Scherman, D. Noncovalent Functionalization of Carbon Nanotubes with Amphiphilic Gd^{3+} Chelates: Toward Powerful T_1 and T_2 MRI Contrast Agents. *Nano Lett.* **2008**, *8*, 232–236. [\[CrossRef\]](#)
60. Rieter, W.J.; Taylor, K.M.L.; An, H.; Lin, W.; Lin, W. Nanoscale Metal–Organic Frameworks as Potential Multimodal Contrast Enhancing Agents. *J. Am. Chem. Soc.* **2006**, *128*, 9024–9025. [\[CrossRef\]](#)
61. Wang, D.; Zhou, J.; Chen, R.; Shi, R.; Zhao, G.; Xia, G.; Li, R.; Liu, Z.; Tian, J.; Wang, H.; et al. Controllable synthesis of dual-MOFs nanostructures for pH-responsive artemisinin delivery, magnetic resonance and optical dual-modal imaging-guided chemo/photothermal combinational cancer therapy. *Biomaterials* **2016**, *100*, 27–40. [\[CrossRef\]](#) [\[PubMed\]](#)
62. Taylor, K.M.L.; Rieter, W.J.; Lin, W. Manganese-Based Nanoscale Metal–Organic Frameworks for Magnetic Resonance Imaging. *J. Am. Chem. Soc.* **2008**, *130*, 14358–14359. [\[CrossRef\]](#) [\[PubMed\]](#)

63. He, M.; Chen, Y.; Tao, C.; Tian, Q.; An, L.; Lin, J.; Tian, Q.; Yang, H.; Yang, S. Mn-Porphyrin-Based Metal–Organic Framework with High Longitudinal Relaxivity for Magnetic Resonance Imaging Guidance and Oxygen Self-Supplementing Photodynamic Therapy. *ACS Appl. Mater. Interfaces* **2019**, *11*, 41946–41956. [[CrossRef](#)] [[PubMed](#)]
64. Mulder, W.J.M.; Strijkers, G.J.; van Tilborg, G.A.F.; Griffioen, A.W.; Nicolay, K. Lipid-based nanoparticles for contrast-enhanced MRI and molecular imaging. *NMR Biomed.* **2006**, *19*, 142–164. [[CrossRef](#)]
65. Magin, R.L.; Wright, S.M.; Niesman, M.R.; Chan, H.C.; Swartz, H.M. Liposome delivery of NMR contrast agents for improved tissue imaging. *Magn. Reson. Med.* **1986**, *3*, 440–447. [[CrossRef](#)]
66. Koenig, S.H.; Brown, R.D.; Kurland, R.; Ohkit, S. Relaxivity and binding of Mn^{2+} ions in solutions of phosphatidylserine vesicles. *Magn. Reson. Med.* **1988**, *7*, 133–142. [[CrossRef](#)]
67. Devoisselle, J.M.; Vion-Dury, J.; Galons, J.P.; Confort-Gouny, S.; Coustaut, D.; Canioni, P.; Cozzone, P.J. Entrapment of Gadolinium-DTPA in Liposomes: Characterization of Vesicles by P-31 NMR Spectroscopy. *Investig. Radiol.* **1988**, *23*, 719–724. [[CrossRef](#)]
68. Tilcock, C.; Unger, E.; Cullis, P.; MacDougall, P. Liposomal Gd-DTPA: Preparation and characterization of relaxivity. *Radiology* **1989**, *171*, 77–80. [[CrossRef](#)]
69. Kabalka, G.W.; Davis, M.A.; Moss, T.H.; Buonocore, E.; Hubner, K.; Holmberg, E.; Maruyama, K.; Huang, L. Gadolinium-labeled liposomes containing various amphiphilic Gd-DTPA derivatives: Targeted MRI contrast enhancement agents for the liver. *Magn. Reson. Med.* **1991**, *19*, 406–415. [[CrossRef](#)]
70. Kabalka, G.W.; Buonocore, E.; Hubner, K.; Davis, M.; Huang, L. Gadolinium-labeled liposomes containing paramagnetic amphiphilic agents: Targeted MRI contrast agents for the liver. *Magn. Reson. Med.* **1988**, *8*, 89–95. [[CrossRef](#)]
71. Trubetsky, V.S.; Cannillo, J.A.; Milshtein, A.; Wolf, G.L.; Torchilin, V.P. Controlled delivery of Gd-containing liposomes to lymph nodes: Surface modification may enhance MRI contrast properties. *Magn. Reson. Imaging* **1995**, *13*, 31–37. [[CrossRef](#)]
72. Bertini, I.; Bianchini, F.; Calorini, L.; Colagrande, S.; Fragai, M.; Franchi, A.; Gallo, O.; Gavazzi, C.; Luchinat, C. Persistent contrast enhancement by sterically stabilized paramagnetic liposomes in murine melanoma. *Magn. Reson. Med.* **2004**, *52*, 669–672. [[CrossRef](#)] [[PubMed](#)]
73. Sipkins, D.A.; Cheres, D.A.; Kazemi, M.R.; Nevin, L.M.; Bednarski, M.D.; Li, K.C. Detection of tumor angiogenesis in vivo by $\alpha v \beta 3$ -targeted magnetic resonance imaging. *Nat. Med.* **1998**, *4*, 623–626. [[CrossRef](#)] [[PubMed](#)]
74. Aryal, M.; Papademetriou, I.; Zhang, Y.Z.; Power, C.; McDannold, N.; Porter, T. MRI Monitoring and Quantification of Ultrasound-Mediated Delivery of Liposomes Dually Labeled with Gadolinium and Fluorophore through the Blood-Brain Barrier. *Ultrasound Med. Biol.* **2019**, *45*, 1733–1742. [[CrossRef](#)] [[PubMed](#)]
75. Qin, J.; Laurent, S.; Jo, Y.S.; Roch, A.; Mikhaylova, M.; Bhujwalla, Z.M.; Muller, R.N.; Muhammed, M.A. High-Performance Magnetic Resonance Imaging T2 Contrast Agent. *Adv. Mater.* **2007**, *19*, 1874–1878. [[CrossRef](#)]
76. Bao, Y.; Sherwood, J.A.; Sun, Z. Magnetic iron oxide nanoparticles as T_1 contrast agents for magnetic resonance imaging. *J. Mater. Chem. C* **2018**, *6*, 1280–1290. [[CrossRef](#)]
77. Tao, C.; Zheng, Q.; An, L.; He, M.; Lin, J.; Tian, Q.; Yang, S. T_1 -Weight Magnetic Resonance Imaging Performances of Iron Oxide Nanoparticles Modified with a Natural Protein Macromolecule and an Artificial Macromolecule. *Nanomaterials* **2019**, *9*, 170. [[CrossRef](#)]
78. Wei, H.; Bruns, O.T.; Kaul, M.G.; Hansen, E.C.; Barch, M.; Wiśniowska, A.; Chen, O.; Chen, Y.; Li, N.; Okada, S.; et al. Exceedingly small iron oxide nanoparticles as positive MRI contrast agents. *Proc. Natl. Acad. Sci. USA* **2017**, *114*, 2325–2330. [[CrossRef](#)]
79. Wang, G.; Zhang, X.; Skallberg, A.; Liu, Y.; Hu, Z.; Mei, X.; Uvdal, K. One-step synthesis of water-dispersible ultra-small Fe_3O_4 nanoparticles as contrast agents for T_1 and T_2 magnetic resonance imaging. *Nanoscale* **2014**, *6*, 2953. [[CrossRef](#)]
80. Illés, E.; Szekeres, M.; Tóth, I.Y.; Farkas, K.; Földesi, I.; Szabó, Á.; Iván, B.; Tombácz, E. PEGylation of Superparamagnetic Iron Oxide Nanoparticles with Self-Organizing Polyacrylate-PEG Brushes for Contrast Enhancement in MRI Diagnosis. *Nanomaterials* **2018**, *8*, 776. [[CrossRef](#)]

81. Pellico, J.; Ruiz-Cabello, J.; Fernández-Barahona, I.; Gutiérrez, L.; Lechuga-Vieco, A.V.; Enríquez, J.A.; Morales, M.P.; Herranz, F. One-Step Fast Synthesis of Nanoparticles for MRI: Coating Chemistry as the Key Variable Determining Positive or Negative Contrast. *Langmuir* **2017**, *33*, 10239–10247. [[CrossRef](#)] [[PubMed](#)]
82. Alipour, A.; Soran-Erdem, Z.; Utkur, M.; Sharma, V.K.; Algin, O.; Saritas, E.U.; Demir, H.V. A new class of cubic SPIONs as a dual-mode T_1 and T_2 contrast agent for MRI. *Magn. Reson. Imaging* **2018**, *49*, 16–24. [[CrossRef](#)]
83. Chan, N.; Laprise-Pelletier, M.; Chevallier, P.; Bianchi, A.; Fortin, M.A.; Oh, J.K. Multidentate block-copolymer-stabilized ultrasmall superparamagnetic iron oxide nanoparticles with enhanced colloidal stability for magnetic resonance imaging. *Biomacromolecules* **2014**, *15*, 2146–2156. [[CrossRef](#)] [[PubMed](#)]
84. Hu, F.; Jia, Q.; Li, Y.; Gao, M. Facile synthesis of ultrasmall PEGylated iron oxide nanoparticles for dual-contrast T_1 - and T_2 -weighted magnetic resonance imaging. *Nanotechnology* **2011**, *22*, 245604. [[CrossRef](#)] [[PubMed](#)]
85. Iqbal, M.Z.; Ma, X.; Chen, T.; Ren, W.; Xiang, L.; Wu, A. Silica-coated super-paramagnetic iron oxide nanoparticles (SPIONPs): A new type contrast agent of T_1 magnetic resonance imaging (MRI). *J. Mater. Chem. B* **2015**, *3*, 5172–5181. [[CrossRef](#)]
86. Jung, H.; Park, B.; Lee, C.; Cho, J.; Suh, J.; Park, J.; Kim, Y.; Kim, J.; Cho, G.; Cho, H. Dual MRI T_1 and $T_2^{(*)}$ contrast with size-controlled iron oxide nanoparticles. *Nanomed. Nanotechnol. Biol. Med.* **2014**, *10*, 1679–1689. [[CrossRef](#)] [[PubMed](#)]
87. Kim, B.H.; Lee, N.; Kim, H.; An, K.; Park, Y.I.; Choi, Y.; Shin, K.; Lee, Y.; Kwon, S.G.; Na, H.B.; et al. Large-scale synthesis of uniform and extremely small-sized iron oxide nanoparticles for high-resolution T_1 magnetic resonance imaging contrast agents. *J. Am. Chem. Soc.* **2011**, *133*, 12624–12631. [[CrossRef](#)]
88. Li, F.; Liang, Z.; Liu, J.; Sun, J.; Hu, X.; Zhao, M.; Liu, J.; Bai, R.; Kim, D.; Sun, X.; et al. Dynamically Reversible Iron Oxide Nanoparticle Assemblies for Targeted Amplification of T_1 -Weighted Magnetic Resonance Imaging of Tumors. *Nano Lett.* **2019**, *19*, 4213–4220. [[CrossRef](#)]
89. Li, P.; Chevallier, P.; Ramrup, P.; Biswas, D.; Vuckovich, D.; Fortin, M.A.; Oh, J.K. Mussel-Inspired Multidentate Block Copolymer to Stabilize Ultrasmall Superparamagnetic Fe_3O_4 for Magnetic Resonance Imaging Contrast Enhancement and Excellent Colloidal Stability. *Chem. Mater.* **2015**, *27*, 7100–7109. [[CrossRef](#)]
90. Li, Z.; Yi, P.W.; Sun, Q.; Lei, H.; Li Zhao, H.; Zhu, Z.H.; Smith, S.C.; Lan, M.B.; Lu, G.Q. Ultrasmall Water-Soluble and Biocompatible Magnetic Iron Oxide Nanoparticles as Positive and Negative Dual Contrast Agents. *Adv. Funct. Mater.* **2012**, *22*, 2387–2393. [[CrossRef](#)]
91. Liu, C.L.; Peng, Y.K.; Chou, S.W.; Tseng, W.H.; Tseng, Y.J.; Chen, H.C.; Hsiao, J.K.; Chou, P.T. One-Step, Room-Temperature Synthesis of Glutathione-Capped Iron-Oxide Nanoparticles and their Application in In Vivo T_1 -Weighted Magnetic Resonance Imaging. *Small* **2014**, *10*, 3962–3969. [[CrossRef](#)] [[PubMed](#)]
92. Luo, Y.; Yang, J.; Yan, Y.; Li, J.; Shen, M.; Zhang, G.; Mignani, S.; Shi, X. RGD-functionalized ultrasmall iron oxide nanoparticles for targeted T_1 -weighted MR imaging of gliomas. *Nanoscale* **2015**, *7*, 14538–14546. [[CrossRef](#)] [[PubMed](#)]
93. Macher, T.; Totenhagen, J.; Sherwood, J.; Qin, Y.; Gurler, D.; Bolding, M.S.; Bao, Y. Ultrathin iron oxide nanowhiskers as positive contrast agents for magnetic resonance imaging. *Adv. Funct. Mater.* **2015**, *25*, 490–494. [[CrossRef](#)]
94. Shen, Z.; Chen, T.; Ma, X.; Ren, W.; Zhou, Z.; Zhu, G.; Zhang, A.; Liu, Y.; Song, J.; Li, Z.; et al. Multifunctional Theranostic Nanoparticles Based on Exceedingly Small Magnetic Iron Oxide Nanoparticles for T_1 -Weighted Magnetic Resonance Imaging and Chemotherapy. *ACS Nano* **2017**, *11*, 10992–11004. [[CrossRef](#)] [[PubMed](#)]
95. Shen, L.H.; Bao, J.F.; Wang, D.; Wang, Y.X.; Chen, Z.W.; Ren, L.; Zhou, X.; Ke, X.B.; Chen, M.; Yang, A.Q. One-step synthesis of monodisperse, water-soluble ultra-small Fe_3O_4 nanoparticles for potential bio-application. *Nanoscale* **2013**, *5*, 2133–2141. [[CrossRef](#)]
96. Taboada, E.; Rodríguez, E.; Roig, A.; Oró, J.; Roch, A.; Muller, R.N. Relaxometric and Magnetic Characterization of Ultrasmall Iron Oxide Nanoparticles with High Magnetization. Evaluation as Potential T_1 Magnetic Resonance Imaging Contrast Agents for Molecular Imaging. *Langmuir* **2007**, *23*, 4583–4588. [[CrossRef](#)]
97. Tromsdorf, U.I.; Bruns, O.T.; Salmen, S.C.; Beisiegel, U.; Weller, H. A Highly Effective, Nontoxic T_1 MR Contrast Agent Based on Ultrasmall PEGylated Iron Oxide Nanoparticles. *Nano Lett.* **2009**, *9*, 4434–4440. [[CrossRef](#)]

98. Vangijzegem, T.; Stanicki, D.; Boutry, S.; Paternoster, Q.; Vander Elst, L.; Muller, R.N.; Laurent, S. VSION as high field MRI T_1 contrast agent: Evidence of their potential as positive contrast agent for magnetic resonance angiography. *Nanotechnology* **2018**, *29*, 265103. [[CrossRef](#)]
99. Fernández-Barahona, I.; Gutiérrez, L.; Veintemillas-Verdaguer, S.; Pellico, J.; Morales MD, P.; Catala, M.; del Pozo, M.A.; Ruiz-Cabello, J.; Herranz, F. Cu-Doped Extremely Small Iron Oxide Nanoparticles with Large Longitudinal Relaxivity: One-Pot Synthesis and in Vivo Targeted Molecular Imaging. *ACS Omega* **2019**, *4*, 2719–2727. [[CrossRef](#)]
100. Yang, L.; Zhou, Z.; Liu, H.; Wu, C.; Zhang, H.; Huang, G.; Ai, H.; Gao, J. Europium-engineered iron oxide nanocubes with high T_1 and T_2 contrast abilities for MRI in living subjects. *Nanoscale* **2015**, *7*, 6843–6850. [[CrossRef](#)]
101. Zeng, L.; Ren, W.; Zheng, J.; Cui, P.; Wu, A. Ultrasmall water-soluble metal-iron oxide nanoparticles as T_1 -weighted contrast agents for magnetic resonance imaging. *Phys. Chem. Chem. Phys.* **2012**, *14*, 2631–2636. [[CrossRef](#)] [[PubMed](#)]
102. Yin, X.; Russek, S.E.; Zabow, G.; Sun, F.; Mohapatra, J.; Keenan, K.E.; Boss, M.A.; Zeng, H.; Liu, P.J.; Viert, A.; et al. Large T_1 contrast enhancement using superparamagnetic nanoparticles in ultra-low field MRI. *Sci. Rep.* **2018**, *8*, 11863. [[CrossRef](#)] [[PubMed](#)]
103. Ali, A.; Hira Zafar, M.Z.; ul Haq, I.; Phull, A.R.; Ali, J.S.; Hussain, A. Synthesis, characterization, applications, and challenges of iron oxide nanoparticles. *Nanotechnol. Sci. Appl.* **2016**, *9*, 49–67. [[CrossRef](#)] [[PubMed](#)]
104. Tao, C.; Chen, Y.; Wang, D.; Cai, Y.; Zheng, Q.; An, L.; Lin, J.; Tian, Q.; Yang, S. Macromolecules with Different Charges, Lengths, and Coordination Groups for the Coprecipitation Synthesis of Magnetic Iron Oxide Nanoparticles as T_1 MRI Contrast Agents. *Nanomaterials* **2019**, *9*, 699. [[CrossRef](#)] [[PubMed](#)]
105. Joseyphus, R.J.; Kodama, D.; Matsumoto, T.; Sato, Y.; Jeyadevan, B.; Tohji, K. Role of polyol in the synthesis of Fe particles. *J. Magn. Magn. Mater.* **2007**, *310*, 2393–2395. [[CrossRef](#)]
106. Hu, F.; MacRenaris, K.W.; Waters, E.A.; Liang, T.; Schultz-Sikma, E.A.; Eckermann, A.L.; Meade, T.J. Ultrasmall, Water-Soluble Magnetite Nanoparticles with High Relaxivity for Magnetic Resonance Imaging. *J. Phys. Chem. C* **2009**, *113*, 20855–20860. [[CrossRef](#)]
107. Fernández-Barahona, I.; Muñoz-Hernando, M.; Herranz, F. Microwave-Driven Synthesis of Iron-Oxide Nanoparticles for Molecular Imaging. *Molecules* **2019**, *24*, 1224. [[CrossRef](#)]
108. Bhavesh, R.; Lechuga-Vieco, A.V.; Ruiz-Cabello, J.; Herranz, F. T_1 -MRI Fluorescent Iron Oxide Nanoparticles by Microwave Assisted Synthesis. *Nanomaterials* **2015**, *5*, 1880–1890. [[CrossRef](#)]
109. Pellico, J.; Ruiz-Cabello, J.; Saiz-Alía, M.; del Rosario, G.; Caja, S.; Montoya, M.; Fernández de Manuel, L.; Morales, M.P.; Gutiérrez, L.; Galiana, B.; et al. Fast synthesis and bioconjugation of ^{68}Ga core-doped extremely small iron oxide nanoparticles for PET/MR imaging. *Contrast Media Mol. Imaging* **2016**, *11*, 203–210. [[CrossRef](#)]
110. Ju, K.Y.; Lee, J.W.; Im, G.H.; Lee, S.; Pyo, J.; Park, S.B.; Lee, J.H.; Lee, J.K. Bio-inspired, melanin-like nanoparticles as a highly efficient contrast agent for T_1 -weighted magnetic resonance imaging. *Biomacromolecules* **2013**, *14*, 3491–3497. [[CrossRef](#)]
111. Peng, Y.K.; Liu, C.L.; Chen, H.C.; Chou, S.W.; Tseng, W.H.; Tseng, Y.J.; Kang, C.C.; Hsiao, J.K.; Chou, P.T. Antiferromagnetic iron nanocolloids: A new generation in vivo T_1 mri contrast agent. *J. Am. Chem. Soc.* **2013**, *135*, 18621–18628. [[CrossRef](#)] [[PubMed](#)]
112. Wu, M.; Meng, Q.; Chen, Y.; Xu, P.; Zhang, S.; Li, Y.; Zhang, L.; Wang, M.; Yao, H.; Shi, J. Ultrasmall confined Iron oxide nanoparticle MSNs as a pH-responsive theranostic platform. *Adv. Funct. Mater.* **2014**, *24*, 4273–4283. [[CrossRef](#)]
113. Li, Z.; Wang, S.X.; Sun, Q.; Zhao, H.L.; Lei, H.; Lan, M.B. Ultrasmall Manganese Ferrite Nanoparticles as Positive Contrast Agent for Magnetic Resonance Imaging. *Adv. Healthc. Mater.* **2013**, *2*, 958–964. [[CrossRef](#)] [[PubMed](#)]
114. Huang, G.; Li, H.; Chen, J.; Zhao, Z.; Yang, L.; Chi, X.; Chen, Z.; Wang, X.; Gao, J. Tunable T_1 and T_2 contrast abilities of manganese-engineered iron oxide nanoparticles through size control. *Nanoscale* **2014**, *6*, 10404–10412. [[CrossRef](#)] [[PubMed](#)]
115. Zhang, M.; Cao, Y.; Wang, L.; Ma, Y.; Tu, X.; Zhang, Z. Manganese doped iron oxide theranostic nanoparticles for combined T_1 magnetic resonance imaging and photothermal therapy. *ACS Appl. Mater. Interfaces* **2015**, *7*, 4650–4658. [[CrossRef](#)] [[PubMed](#)]
116. Lee, N.; Yoo, D.; Ling, D.; Cho, M.H.; Hyeon, T.; Cheon, J. Iron Oxide Based Nanoparticles for Multimodal Imaging and Magnetoresponsive Therapy. *Chem. Rev.* **2015**, *115*, 10637–10689. [[CrossRef](#)] [[PubMed](#)]

117. Pellico, J.; Fernández-Barahona, I.; Benito, M.; Gaitán-Simón, Á.; Gutiérrez, L.; Ruiz-Cabello, J.; Herranz, F. Unambiguous detection of atherosclerosis using bioorthogonal nanomaterials. *Nanomed. Nanotechnol. Biol. Med.* **2019**, *17*, 26–35. [[CrossRef](#)]
118. Sandiford, L.; Phinikaridou, A.; Protti, A.; Meszaros, L.K.; Cui, X.; Yan, Y.; Frodsham, G.; Williamson, P.A.; Gaddum, N.; Botnar, R.M.; et al. Bisphosphonate-anchored pegylation and radiolabeling of superparamagnetic iron oxide: Long-circulating nanoparticles for in vivo multimodal (T_1 MRI-SPECT) imaging. *ACS Nano* **2013**, *7*, 500–512. [[CrossRef](#)]
119. Wang, G.; Gao, W.; Zhang, X.; Mei, X. Au Nanocage Functionalized with Ultra-small Fe_3O_4 Nanoparticles for Targeting T_1 – T_2 Dual MRI and CT Imaging of Tumor. *Sci. Rep.* **2016**, *6*, 28258. [[CrossRef](#)]
120. Pellico, J.; Ellis, C.M.; Davis, J.J. Nanoparticle-Based Paramagnetic Contrast Agents for Magnetic Resonance Imaging. *Contrast Media Mol. Imaging* **2019**, 2019, 1845637. [[CrossRef](#)]



© 2020 by the authors. Licensee MDPI, Basel, Switzerland. This article is an open access article distributed under the terms and conditions of the Creative Commons Attribution (CC BY) license (<http://creativecommons.org/licenses/by/4.0/>).